Requirements for development of T-helper1 and T-follicular helper cells from a common precursor

Douwe M. T. Bosma[1,2*], Julia Busselaar[1,2*], Mo D. Staal[1,2], Mylene de Koning[1], Xin Lei[1,2], Tom de Wit[1,2], Yanling Xiao[1,2], Jannie Borst[1,2**] and Fiamma Salerno[1**]

[1]Department of Immunology and [2]Oncode Institute, Leiden University Medical Center, 2333 ZA Leiden, The Netherlands

*Shared first authors

**Shared last authors

Correspondence to: f.salerno@lumc.nl & j.g.borst@lumc.nl

Lead contact: j.g.borst@lumc.nl

Authors ORCID: D.M.T.B: 0000-0002-3500-8649; J.Bu: 0000-0003-2402-4245; M.D.S: 0000-0001-8568-6248; M. K: 0009-0005-5323-5983; T.d.W: 0009-0001-4082-2805; Y.X: 0000-0003-1755-1709; J.Bo: 0000-0002-8043-5009; F.S: 0000-0002-8595-4051

Summary

Activated CD4 T cells become either T-helper (Th) or T-follicular helper (Tfh) cells that support cellular or humoral immunity. We have investigated how polyclonal, vaccine induced T cells in mice bifurcate into Th1- and Tfh trajectories. We show that Th1 and Tfh cells originate from the same, highly proliferative precursor clones that co-express Th1- and Tfh-related transcription factors and chemokine receptors, including T-bet, BCL6, CXCR3 and CXCR5. Generation of the common Th1/Tfh precursor pool from antigen-specific CD4 T cells relies on CD28 costimulation but occurs independently of type-1 conventional dendritic cells (cDC1s) or B cells. Differentiation of Th1/Tfh precursors into the Th1 lineage relies on CD40 costimulation and cDC1s, while differentiation into the Tfh lineage relies on ICOS costimulation and B cells. Thus, activated CD4 T cells give rise to a bipotent Th1/Tfh precursor and differentiation into Th1 or Tfh cells depends on interactions with antigen-presenting cDC1s or B cells.

Keywords:
CD4 T cell, T-cell differentiation, T-helper 1, T-follicular helper, vaccination, costimulation, cDC1, B cell

Introduction

Upon antigen encounter within secondary lymphoid organs, CD4 T cells are activated, clonally expand and initiate differentiation into T-helper (Th)1, 2 or 17 lineages to regulate cellular immunity (Yin et al., 2021). At the same time, T-follicular helper (Tfh) cells are formed, which promote B-cell expansion and differentiation in germinal centers (GC) (Vinuesa et al., 2016). During a type-I immune response, Th1 and Tfh cells emerge in parallel, suggesting a bifurcation in their effector differentiation trajectories (Duckworth & Groom, 2021; Lönnberg et al., 2017; Osum & Jenkins, 2023). This process is not exclusive of type-I responses, as Tfh cells are likewise generated in parallel with Th2 or Th17 effector CD4 T cells (Eisenbarth et al., 2021; Künzli & Masopust, 2023). Coordination of cell-mediated and humoral immunity thus depends on Th/Tfh lineage decision making in activated CD4 T cells. This process is a potential target for therapeutic intervention e.g. in vaccination, cancer and auto-immunity.

Effector CD4 T-cell differentiation relies on successive interactions with different professional antigen-presenting cells (APCs) and is initiated upon cognate contact with conventional dendritic cells (cDCs). Among these, the cDC2 lineage excels at (soluble) antigen presentation in major histocompatibility complex (MHC)-II molecules (Dudziak et al., 2007) and are important for initial CD4 T-cell activation (De Giovanni et al., 2020; Hilligan & Ronchese, 2020). The cDC1 lineage is much more proficient in phagocytosing cell-bound antigen and cross-presenting this in MHC-I molecules, thus playing a crucial role in CD8 T-cell activation (Den Haan et al., 2000; Hildner et al., 2008; Martínez-López et al., 2015). cDC1s can also contribute to CD4 T cell priming (Ferris et al., 2020; Wu & Murphy, 2022) and relay help for effector and memory differentiation of CD8 T cells (Borst et al., 2018; Lei et al., 2024). In contrast, B cells are considered essential APCs to promote CD4 T-cell differentiation into Tfh cells (Crotty, 2014; Lönnberg et al., 2017).

In general, effector differentiation of CD4 T cells is guided by the activation and maturation state of cDCs and B cells, which are reflected in their costimulatory and cytokine profiles (De Giovanni et al., 2020; Künzli & Masopust, 2023; Yin et al., 2021). These inputs, as delivered during multiple sequential interactions between T cells and APCs collectively regulate expression of lineage-determining transcription factors that direct Th differentiation along specific trajectories. Decision-making between Th and Tfh lineage commitment likewise depends on certain lineage-defining transcription factors. Whereas transient co-expression of T-bet and BCL6 has been reported in *in vitro* T-cell cultures (Nakayamada et al., 2011), *in vivo* studies indicate that the choice between Th1 and Tfh cell differentiation depends on the ratio of T-bet versus BCL6 protein levels, which is

determined by initiation of negative regulatory circuits. For example, BCL6 represses genes encoding Th1, Th2 and Th17 lineage-specific transcription factors, including *Tbx21* (encoding T-bet), *Gata3* and *Rora* (J. Choi et al., 2020). However, when it binds to T-bet, BCL6 can no longer repress the *Prdm1* gene encoding BLIMP1. As a result, BLIMP1 starts to suppress Tfh-associated genes, thus favoring Th1 differentiation (Oestreich et al., 2012). In contract, transient early T-bet expression is required for upregulation of CXCR5 and generation of IFNγ-producing Tfh cells in response to infection (Fang et al., 2018; Weinstein et al., 2018).

In this paper, we address the mechanisms underlying bifurcation of the Th1 and Tfh lineages. The CD4 T-cell differentiation trajectories leading to these cell fates have generally been studied separately (Osum & Jenkins, 2023). Also, they have primarily focused on T cell receptor (TCR)-transgenic CD4 T cells (Cho et al., 2017; Fazilleau et al., 2009; Lönnberg et al., 2017; Tubo et al., 2013) and not yet revealed the bifurcation process during endogenous, polyclonal CD4 T-cell responses (Künzli & Masopust, 2023). This is a relevant distinction since TCR affinity has been proposed to impact the differentiation trajectories in some studies (Fazilleau et al., 2009; Künzli et al., 2021; Tubo et al., 2013), but not in others (Cho et al., 2017; De Giovanni et al., 2020). Deconvolution of CD4 T-cell differentiation pathways can be challenging due to high plasticity of CD4 T-helper lineages (Alterauge et al., 2020; O'Shea & Paul, 2010) and stochastic events (Kiner et al., 2021).

Different lines of evidence point to the existence of a common precursor of Th1 and Tfh cells. Single cell RNA-sequencing (scRNAseq) of antigen-specific TCR transgenic PbTII CD4 T cells to *Plasmodium chabaudi* revealed that prior to Th1 or Tfh differentiation, CD4 T cells attain a common activated precursor state co-expressing *Cxcr5* and *Cxcr3* mRNA (Lönnberg et al., 2017). In lymphocytic choriomeningitis virus (LCMV), a memory-like CD4 precursor was found to be clonally related to Th1 and Tfh cells (Xia et al., 2022). Understanding whether and how overlapping Th1/Tfh intermediate cell states arise in normal polyclonal responses is critical, as these cells represent a promising target to therapeutically direct Th1 or Tfh differentiation in disease. Defining the signals that bias differentiation toward either lineage is therefore essential. These precursors also hold potential as prognostic or predictive markers and for immunomonitoring of treatment responses.

Here, we used a mouse vaccination model to induce and trace the differentiation trajectories of endogenous CD4 T cells in healthy mice. By combining high-dimensional flow cytometry, single-cell RNA-sequencing (scRNAseq) and TCR-sequencing, we identified that antigen-specific CD4 T clones pass through a bipotent Th1/Tfh precursor state, before committing to a specific differentiation trajectory. We identify the gene

90 and protein expression profile of this precursor and extrapolate its existence to mouse infection settings. We
91 also define key costimulatory signals and interactions with APCs that guide differentiation commitment of the
92 Th1/Tfh precursor to either the Th1 or Tfh lineage.

93

94 Results

95 **Vaccination raises endogenous, functional Th1 and Tfh cells in equal measure.**

96 To study how endogenous CD4 T cells differentiate *in vivo*, we used a mouse vaccination model that has
97 previously revealed the effects of CD4 T-cell help on effector and memory CD8 T-cell differentiation (Ahrends
98 et al., 2016, 2017, 2019). In this model, we vaccinate C57BL/6 mice with plasmid DNA encoding an
99 immunodominant MHC-I (H-2D^{b}) restricted epitope E7$_{48-57}$ from human papilloma virus (HPV) either alone
100 (Control) or linked to three MHC-II-restricted helper epitopes: p30, PADRE, and NEF (MHC-II) (**Figure 1A**).
101 These MHC-II-restricted epitopes were selected for binding to human HLA-DP, -DQ and -DR, respectively
102 (Oosterhuis et al., 2012), but p30 and PADRE can also be presented by MHC-II (I-A^{b}) (Alexander et al., 1994;
103 Rice et al., 2001) and prime CD4 T-cell responses in mice (Ahrends et al., 2016; Bosma et al., 2025). The
104 plasmid DNA vaccine is “tattooed” into the depilated skin of the hind leg and expressed in keratinocytes, followed
105 by antigen delivery to the draining lymph node (dLN) by cDCs and by passive drainage (Babała et al., 2018;
106 Bins et al., 2005). The antigen-specific CD4 T-cell response can be followed by flow cytometry using an MHC-
107 II tetramer (tet) against the PADRE epitope (**Figure 1B**). PADRE tet^{+} CD4 T cells were detected in the dLN from
108 day 4 onwards after vaccination (**Figure 1C**) and entered the circulation by day 5 (**Supplementary Figure 1A**).
109 In line with a type-1 immune response raised by this model, PADRE tet^{+} cells differentiated into Th1 and Tfh
110 cells, and did not differentiate into T-regulatory (Treg), Th2 or Th17 cells (**Supplementary Figure 1B)**. Among
111 PADRE tet^{+} CD4 T cells, Th1 cells were defined by PSGL1, T-bet and SLAM coexpression and low or no TCF1
112 expression (**Figure 1D; Supplementary Figure 1C**) (Marshall et al., 2011; Shaw et al., 2016; Zou et al., 2024).
113 Conversely, Tfh cells were defined by low or no PSGL1, T-bet and SLAM expression, gain of CXCR5, BCL6,
114 PD-1 and maintained TCF1 expression (**Figure 1D**) (Y. S. Choi et al., 2015; Künzli & Masopust, 2023; Marshall
115 et al., 2011; Osum & Jenkins, 2023). Th1 and Tfh populations emerged in parallel and were of similar size at
116 day 4 after vaccination (**Figure 1E**). By day 5, when PADRE tet^{+} CD4 T cells became detectable in the blood
117 (**Supplementary Figure 1A**), Tfh cells started accumulating in the dLN (**Figure 1E**). At that day, Th1 cells went
118 from the dLN to the blood, where they represented ~50% of PADRE^{+} CD4 T cells (**Figure 1F**).

119 To validate the helper functions of Th1 and Tfh cells, we investigated the CD8 T-cell and B-cell
120 responses post vaccination. Mice in which CD4 T cells were activated by the MHC-II vaccine displayed an
121 increased frequency of KLRG1$^+$ effector phenotype E7 tetramer$^+$ CD8 T cells at day 10 in the blood compared
122 to mice receiving the control vaccine (**Figure 1G; Supplementary figure 1D**). These data confirm that the Th1
123 cells generated by the MHC-II vaccine contributed to effector differentiation of the CD8 T cells raised by the E7
124 epitope, as demonstrated before (Ahrends et al., 2016, 2017). Mice that received the MHC-II vaccine also
125 displayed increased frequencies of FAS$^+$ GL7$^+$ germinal center (GC) B cells and CD138$^+$ TACI$^+$ plasmablasts
126 (**Figure 1H; Supplementary Figure 1E-F**), confirming that vaccine-primed Tfh cells promoted the B-cell
127 response. Thus, both Th1 and Tfh cells raised by the MHC-II vaccine are functionally competent. Inhibition of
128 T-cell egress from the dLN with sphingosine 1-phosphate (S1P) receptor-targeting drug FTY720 increased the
129 overall frequency of PADRE tet$^+$ CD4 T cells in the dLN by more than 2-fold (**Supplementary Figure 1G, H**). At
130 day 7 after vaccination, PADRE tet$^+$ Th1 and Tfh cell frequencies and absolute numbers were comparable in
131 dLN of FTY720-treated mice (**Figure 1I; Supplementary Fig 1I**). This finding indicates that the MHC-II vaccine
132 leads in equal measure to Th1 and Tfh differentiation and therefore is a good model to study the differentiation
133 trajectories of the endogenous vaccine-specific CD4 T cells raised.

134

135 **Reconstruction of the Th1- and Tfh differentiation trajectories that evolve after vaccination.**

136 To gain insight into the temporal changes that CD4 T cells undergo during Th1 and Tfh differentiation, we
137 analyzed PADRE tet$^+$ CD4 T cells in the dLNs of mice from day 4 to 9 after vaccination by spectral flow cytometry
138 and dimension reduction analysis (**Figure 2A; Supplementary Figure 2A**). To ensure that we captured the full
139 differentiation trajectory, we gated on total CD4$^+$ PADRE tet$^+$ cells, which include a small proportion of CD62L^{hi}
140 CD44^{low} naïve cells. Indeed, PADRE tet$^+$ CD4 T cells were discriminated into naïve CD62L^{hi} CD44^{low} and
141 activated CD44^{hi} cells (**Figure 2B**). The marker profile of the activated PADRE$^+$ CD4 T-cell pool underwent daily
142 remodeling and displayed progressive branching towards two end points (**Figure 2A; Supplementary Figure**
143 **2A**), which were characterized by a Th1 (PSGL1$^+$ T-bet$^+$ SLAM$^+$ TCF1$^-$ SLAMF6$^-$) or a Tfh (CXCR5$^+$ PD-1$^+$
144 BCL6$^+$ TCF1$^+$ SLAMF6$^+$ FR4$^+$) phenotype (**Figure 2C-E**), as we had observed before (**Figure 1D**). To
145 reconstruct the temporal evolution of PADRE tet$^+$ CD4 T-cell differentiation towards Th1 and Tfh states, we used
146 Wishbone, an algorithm that orders cells according to their developmental progression and infers branching
147 trajectories into only one of two possible fates (Setty et al., 2016). Wishbone calculates differentiation

trajectories based on the rise and fall of phenotypic markers and uses nearest-neighbor graphs to capture developmental distance from a starting point, which we defined as the CD62L^{hi} CD44^{low} naive CD4 T-cell state.

In our experimental setup, PADRE tet^{+} CD4 T cells were ordered based on early activation (CD44, CD62L) and stem-like markers (TCF1, SLAMF6) and the acquisition of the Th1 or Tfh phenotype (Y. S. Choi et al., 2015; Kageyama et al., 2012; Künzli et al., 2020; Marshall et al., 2011; Osum & Jenkins, 2023; Shaw et al., 2016; Zou et al., 2024). PADRE tet^{+} CD4 T cells were positioned along either the trunk or one of the two possible branches of the trajectory (**Figure 2F; Supplementary Figure 2B**). Wishbone identified PSGL1^{+} T-bet^{+} SLAM^{+} Th1 cells as branch 1 and CXCR5^{+} PD-1^{+} BCL6^{+} TCF1^{+} FR4^{+} Tfh cells as branch 2 (**Figure 2C-F**). In contrast, the trunk of the Wishbone trajectory was composed of CD62L^{hi} CD44^{low} naive cells and CD62L^{hi} CD44^{hi} activated cells (**Figure 2B, F**). The CD44^{hi} CD62L^{hi} cells expressed high levels of TCF1 and SLAMF6 (**Figure 2C**), which are considered markers of stem-like CD8 T cells and stem-like Th1 precursors (Busselaar et al., 2020; Cardenas et al., 2024; Zou et al., 2024), thus suggesting the potential of CD44^{hi} CD62L^{hi} cells for further differentiation. In addition, CD44^{hi} CD62L^{hi} cells in the trunk of the trajectory had higher levels of CXCR5, BCL6 and PD-1 compared to naive cells, but still expressed PSGL1 (**Figure 2D, E**)**.** Apart from being highly expressed by Tfh cells, PD-1 is also upregulated as a result of TCR triggering (Agata et al., 1996; Baumeister et al., 2016), and in line with this, all CD44^{hi} cells had higher expression of PD-1 compared to naïve, CD44^{lo} cells (**Figure 2E**). We also show that the pseudotime calculated by Wishbone matched real-time differentiation, as visualized by the decrease in frequency of CD62L^{hi} CD44^{low} and CD62L^{hi} CD44^{hi} cells over time (**Supplementary Figure 2A, C**). Altogether, these data indicate that, upon activation, antigen-specific CD4 T cells pass through a common CD44^{hi} CD62L^{hi} cell state before branching into Th1 or Tfh differentiation states.

Th1 and Tfh cells develop from common precursor clones according to single-cell TCR sequencing.

To characterize CD4 T-cell differentiation trajectories in an unbiased manner, we performed scRNAseq and paired TCRseq. For this purpose, mice received the MHC-II vaccine and CD3^{+} CD44^{hi} CD62L^{low} T cells were flow cytometrically purified from the dLN at days 5 or 10 after vaccination (**Supplementary Figure 3A**). After quality control filtering, selection of cells co-expressing TCRα and TCRβ sequences and exclusion of CD8 T cells and γδT cells (**Supplementary Figure 3B**), we obtained 4656 CD4 T cells for data analysis. Dimensionality reduction and clustering of cells based on their gene expression profiles identified 7 clusters that contained more than 20 cells (**Figure 3A, B; Supplementary Figure 3C**). Clusters 0 and 4 identified two Treg cell

177 populations, characterized by expression of *Foxp3*, *Ctla4* and *Il2ra* (encoding CD25) (**Figure 3C**). Cluster 1
178 identified Tfh cells expressing *Tcf7* (encoding TCF1), *Cxcr5*, *Bcl6* and *Pdcd1* (encoding PD-1); cluster 2
179 identified Th1 cells expressing *Selplg* (encoding PSGL1), *Tbx21* (encoding T-bet), *Id2*, and *Cxcr3*; cluster 3
180 identified naive-like cells expressing *Ccr7*, *Lef1*, *Sell* (encoding CD62L), and *Tcf7*; whereas cluster 6 was
181 dominated by an interferon (IFN)-stimulated gene (ISG) signature (**Figure 3C**). Interestingly, cluster 5 contained
182 cells expressing both Th1-related genes (*Tbx21*, *Cxcr3*) and Tfh-related genes (*Tcf7*, *Cxcr5*, *Bcl6*, *Pdcd1*)
183 (**Figure 3C**). The expression levels of these genes were intermediate between those found in Th1 cells (cl. 2)
184 and Tfh cells (cl. 1). Cells of cluster 5 also expressed *Pdcd1* and *Cd69*, which are also markers of recent TCR
185 triggering (**Figure 3C**) (Agata et al., 1996; Baumeister et al., 2016; Cibrián & Sánchez-Madrid, 2017; Simms &
186 Ellis, 1996). Cluster 5 cells were higher in frequency at day 5 after vaccination than at day 10, supporting that
187 they represent recently activated cells (**Figure 3B**). The frequency of Th1 cells (cl. 2) and Tfh cells (cl. 1) on the
188 other hand, increased over time (**Figure 3B**), which aligns with ongoing effector differentiation of the activated
189 CD4 T-cell pool.

190 Next, to define clonal relationships between CD4 responder T cells in different states of effector
191 differentiation, we paired the gene expression profiles per cell with TCRα and TCRβ sequence information. TCR
192 clones were defined based on identical TCRα and TCRβ complementarity region (CDR)3 sequences, which
193 identified a total number of 3549 clones within the CD4 T-cell compartment. We noted that Tfh cluster 1, Th1
194 cluster 2 and the intermediate phenotype cluster 5 had the highest frequency of expanded clones (>1 cell per
195 clone) among all clusters (**Figure 3D)**. Additionally, the highest number of expanded clones was observed in
196 Tfh cluster 1, followed by Th1 cluster 2, intermediate phenotype cluster 5 and Treg cluster 1 (**Supplementary**
197 **Figure 3D, E**). Out of 352 expanded clones, 171 clones were shared between two or more clusters, while the
198 rest was uniquely expanded within one cluster (**Supplementary Figure 3D**). Tregs of cluster 0 comprised more
199 unique than shared clones and sharing occurred primarily with Tregs of cluster 4 (**Figure 3E, Supplementary**
200 **Figure 3D**). The majority (72%) of expanded clones was shared between Tfh and Th1 cells (cl. 1 and 2), Tfh or
201 Th1 cells and intermediate phenotype cells (cl. 5), or all three populations (**Figure 3E**). Accordingly, at days 5
202 and 10 after vaccination, TCR clonotype sharing between cluster 5 cells and Th1 cells, Tfh cells, or both was
203 evident (**Figure 3F**). These data demonstrate the clonal relationship between cluster 5 cells and Th1 and Tfh
204 cells, and confirm the indication of Wishbone analysis (**Figure 2F**) that antigen-activated CD4 T cells acquire
205 an intermediate differentiation state expressing both Th1 and Tfh-related genes from which they can further
206 develop into committed Th1 or Tfh cells. Cluster 5 cells thus represent the common precursors of Th1 and Tfh

207 lineages. To determine whether Th1/Tfh precursor cells were formed not only after vaccination but also after
208 infection, we used a published dataset of polyclonal GP66-tetramer^{+} antigen-specific CD4 T cells from mice
209 infected with either acute LCMV-Armstrong or chronic LCMV-clone 13 (Xia et al., 2022) (**Figure 3G**). We aligned
210 the transcriptional profile of Tfh (cluster 1), Th1 (cluster 2) and Th1/Tfh precursor cells (cluster 5) as defined in
211 our vaccination setting with this dataset using module scoring. After LCMV infection, Tfh and two Th1 clusters
212 were detected (**Supplementary Figure 4A, B**), with Th1 cells being prominent at day 8 in both infection models,
213 and Tfh cells at day 21 (**Figure 3G**). The two Th1 clusters expressed classical Th1-associated genes including
214 *Cxcr6, Tbx21, Id2,* and *Prf1,* but were distinguished by expression of either *Gzma* and *Gzmb* (Th1 Gzmb^{+}
215 cluster) or *Prdm1, Eomes*, and *Gzmk* (Th1 Prdm1^{+} cluster) (**Supplementary Figure 4E)**. The Tfh cluster
216 expressed characteristic genes including *Cxcr5, Pdcd1, Il21 and Bcl6* (**Supplementary Figure 4E**). Importantly,
217 at day 8 post infection with both acute and chronic LCMV, a population was enriched that matched the Th1/Tfh
218 precursor cluster from our vaccination setting (**Figure 3G, Supplementary Figure 4C**). These cells expressed
219 canonical Th1- and Tfh-associated genes (*Cxcr3*, *Cxcr5, Tbx21, Bcl6*) alongside key markers of the activated
220 memory-precursor cell population described by (Xia et al., 2022) (*Tcf7, Slamf6, Batf, Zbtb32, Mif, Srm, Eif5a,*
221 *Ncl, Hspd1*) (**Supplementary Figure 4E**). We also identified the previously described *Slamf6*$^{+}$ *Tcf7*$^{+}$ *Bcl6*^{lo}
222 memory-precursor cluster (Cardenas et al., 2024; Xia et al., 2022) to be specifically enriched at day 21 post-
223 chronic LCMV infection. Despite the difference in their expression kinetics, the memory-precursor cluster shared
224 features with the Th1/Tfh precursor cluster within the same dataset (**Figure 3G, Supplementary Figure 4D,**
225 **4E**). Altogether, these findings demonstrate that both after vaccination and virus infection, CD4 T cells transit
226 through a common, uncommitted Th1/Tfh precursor state before diverging into Th1 and Tfh cells.

227

228 **Th1/Tfh precursors are proliferative and co-express Th1- and Tfh-related transcription factors and**
229 **chemokine receptors.**

230 To gain deeper insights into the transcriptional programs underlying Th1 and Tfh cell differentiation, we
231 performed differential gene expression analysis between Tfh (cl.1) and Th1 (cl.2) cells generated after
232 vaccination. Gene signatures of the two T-helper subsets were characterized by lineage defining transcription
233 factors, including *Tbx21*, *Id2*, *Bhlhe40* and *Prdm1* for Th1 cells, and *Bcl6*, *Tox* and *Tox2* for Tfh cells, which
234 validated the robustness of our dataset (**Figure 4A**) (Nguyen et al., 2024; Oestreich et al., 2012; Shaw et al.,
235 2016; Xu et al., 2019). Comparison of the transcriptional profile of the common Th1/Tfh precursor cells (cl. 5) to
236 that of naive-like cells (cl. 3) revealed the characteristics of this population (**Figure 4B**). Cluster 5 cells expressed

237 many genes associated with either Th1 or Tfh fate, including transcription factors *Tbx21*, *Bhlhe40*, *Prdm1* and
238 *Bcl6*, as well as chemokine receptors *Cxcr3* and *Cxcr5*. These transcripts were co-expressed within the same
239 cells and enriched in cluster 5 at day 5 post-vaccination, as shown by the positive correlation in expression of
240 e.g. *Tbx21* and *Cxcr5*, or *Tbx21* and *Bcl6* (**Supplementary Figure 5A, B**). In addition, cells of cluster 5 displayed
241 upregulation of *Mki67*, indicating active cell division, and multiple costimulatory receptors including *Icos*, *Tnfrsf8*
242 (encoding CD30), *Tnfrsf9* (encoding CD137, alias 4-1BB), *Tnfrsf18* (encoding CD357, alias GITR), and *Tnfrsf1b*
243 (encoding CD120b, alias TNFR2) (**Figure 4B)**. They also gained expression of the metabolic enzyme lactate
244 dehydrogenase (*Ldha*) (**Figure 4B**), which has been associated with the formation of stem-like Th1 precursors
245 (Zou et al., 2024).

246 To map the formation and function of common Th1/Tfh precursor cells by flow cytometry, we followed
247 the response of TCR transgenic OTII cells that recognize $OVA_{323-339}$ peptide in the context of MHC-II. CD45.1$^+$
248 OTII cells were labeled with carboxyfluorescein succinimidyl ester (CFSE) to track proliferation and adoptively
249 transferred into CD45.2$^+$ recipient mice. One day later, recipient mice received a modified MHC-II DNA vaccine
250 encoding both PADRE and $OVA_{323-339}$ epitopes (MHC-II:OVA; **Supplementary Figure 5C**). This vaccine
251 simultaneously induced an OTII T-cell response to the OVA epitope and an endogenous CD4 T-cell response
252 to the PADRE epitope (**Supplementary Figure 5D, E**), enabling us to compare the differentiation trajectories
253 of these two responder cell populations. Because the transferred naïve OTII cells have a relatively high
254 frequency, this system allowed us to analyze their early activation state at day 3 post-vaccination. Endogenous
255 PADRE tet$^+$ CD4 T cells became detectable by tetramer staining at day 4 post-vaccination (**Supplementary**
256 **Figure 5F, G**) and we therefore monitored the CD4 T-cell response in the dLNs from day 1 to 5 after vaccination.
257 At day 3, OTII cell proliferation was initiated and at day 4, the majority of OTII cells were actively dividing, with
258 a proportion having undergone at least seven divisions already (**Figure 4C, Supplementary Figure 5H**).
259 Accordingly, the frequencies of both OTII cells and PADRE tet$^+$ CD4 T cells were significantly increased by day
260 4 post-vaccination (**Supplementary Figure 5F, G**). At day 3, concurrent with the start of cell division, OTII cells
261 upregulated the activation marker CD44, as well as the chemokine receptor CXCR5 (**Figure 4D,**
262 **Supplementary Fig 5I**) that is commonly used as a marker of Tfh precursors (Baumjohann et al., 2011; Y. S.
263 Choi et al., 2011; Ma et al., 2012). Interestingly, CD44^{hi} CXCR5$^+$ OTII cells also expressed high levels of CXCR3
264 (**Figure 4E, F**), a chemokine receptor that among CD4 T cells is thought to be specifically upregulated on Th1
265 precursors (Ditoro et al., 2018). Consistent with our scRNAseq data, CD44^{hi} CXCR5$^+$ CXCR3$^+$ OTII cells co-
266 expressed T-bet and BCL6 proteins (**Figure 4G, H**). Within the endogenous CD4 T-cell pool, PADRE tet$^+$ CD44^{hi}

267 CD4 T cells also co-expressed CXCR5, CXCR3, T-bet and BCL6 at day 4 post-vaccination (**Figure 4E, G;**
268 **Supplementary Figure 5J-L**). Furthermore, $CD44^{hi}$ OTII cells expressed significantly higher levels of PD-1
269 compared to $CD44^{lo}$ cells (**Supplementary figure 5M**), consistent with our results for endogenous cells (**Figure**
270 **2E; Figure 3C**). TCR transgenic T cells all have the same affinity and may therefore have an intrinsic
271 predisposition to a specific differentiation trajectory (Künzli & Masopust, 2023). Next to low affinity OTII cells,
272 we therefore also used SMARTA T cells that have a high affinity TCR recognizing the GP_{61-80} epitope of LCMV
273 in the context of MHC-II (Ditoro et al., 2018) in conjunction with a modified MHC-II vaccine that encodes both
274 the PADRE and GP_{61-80} epitopes (**Supplemental Figure 5N and O**). SMARTA CD4 T cells also differentiated
275 into $CD44^{+}$ precursor cells co-expressing CXCR3, CXCR5, T-bet and BCL6, as observed at day 4 post-
276 vaccination (**Supplemental Figure 5O**). Obtaining the same results with low and high affinity TCR transgenic
277 CD4 T cells, as well as PADRE-specific endogenous, polyclonal CD4 T cells indicates that the formation of the
278 Th1/Tfh precursor cell pool of this specific phenotype is independent of TCR affinity. The collective data establish
279 that activated CD4 T cells initially form a proliferative pool of bipotent Th1/Tfh precursors with a distinct marker
280 profile that can differentiate into either Th1 or Tfh cells, independent of TCR affinity.

281

282 **Specific costimulatory signals driving formation of the common Th1/Tfh precursor pool and subsequent**
283 **Th1- or Tfh differentiation.**

284 Having identified the common Th1/Tfh precursor, we were interested in the costimulatory signals that drive its
285 formation and further differentiation. It is known that Th1 and Tfh differentiation rely on specific costimulatory
286 signals (Schorer et al., 2019), but the impact of these has not previously been mapped in the differentiation
287 trajectory that we have established here. We first examined the impact of costimulatory receptor CD28 that
288 synergizes with the TCR/CD3 complex in initiating T-cell activation, but reportedly is also required to maintain
289 both Th1 and Tfh cells (Linterman et al., 2014). Mice received OTII cells and MHC-II:OVA-based vaccination
290 and CD28 costimulation was inhibited by infusion of blocking monoclonal antibodies (mAbs) to both CD80 and
291 CD86. This intervention did not significantly affect the overall frequency of OTII cells in dLN at day 5 after
292 vaccination (**Supplementary Figure 6A**), but did reduce the frequency of $CD44^{+}$ $CXCR3^{+}$ $CXCR5^{+}$ OTII Th1/Tfh
293 precursor cells (**Figure 5A**). CD80 and CD86 blockade also reduced the frequency of total PADRE tet^{+} CD4 T
294 cells (**Figure 5B**), thus showing that CD28 costimulation promotes formation of the Th1/Tfh precursor pool by
295 supporting clonal expansion. Because CD80 and CD86 have different affinities for CD28 (Collins et al., 2002)
296 and distinct roles in the maturation of Tfh cells in GCs (Wang et al., 2015), we also investigated whether they

297 had independent impact on the CD4 T-cell differentiation trajectory. Single blockade of either CD80 or CD86 did
298 not affect the generation of CXCR3$^+$ CXCR5$^+$ OTII Th1/Tfh precursor cells (**Figure 5C**), nor the expansion and
299 initial Th1 or Tfh bifurcation of PADRE$^+$ CD4 T cells (**Figure 5D; Supplementary Figure 6B-D**), indicating that
300 CD80 and CD86 are redundant in promoting formation of the Th1/Tfh precursor pool.

301 We next evaluated the impact of CD40 and ICOS costimulation on the CD4 T-cell differentiation
302 trajectory. CD40:CD40L interaction has been reported to promote both Th1 and Tfh function (Baumjohann et
303 al., 2013; Grewal et al., 1995; Liu et al., 2014) and ICOS:ICOSL interaction is important for Tfh differentiation
304 (Baumjohann et al., 2013; Y. S. Choi et al., 2011; Liu et al., 2014; Shin et al., 2015). Blockade of CD40L or
305 ICOSL did not affect the frequency of CD44$^+$ CXCR5$^+$ CXCR3$^+$ OTII precursor cells, total PADRE tet$^+$ CD4 T
306 cells, or total OTII cells (**Figure 5E; Supplementary Figure 6E-F**), indicating that CD40- and ICOS
307 costimulation were not required for formation of the Th1/Tfh precursor pool. However, among PADRE tet$^+$ cells,
308 CD40L blockade significantly reduced the frequency of Th1 cells, while not affecting the frequency of Tfh cells
309 (**Figure 5F-G**). Conversely, blockade of ICOSL lowered the frequency of Tfh cells, while not affecting the
310 frequency of Th1 cells (**Figure 5F, G**). Altogether, these data provide a scenario wherein CD28 costimulation
311 driven by either CD80 or CD86 promotes formation of the Th1/Tfh precursor cell pool, whereafter the precursors
312 are driven into Th1 cells with the aid of CD40-CD40L interactions and into Tfh cells with the aid of ICOS-ICOSL
313 interactions.

314

315 **Th1/Tfh precursors differentiate into either Th1 or Tfh cells in a second priming step on cDC1s or B**
316 **cells, respectively.**

317 We next examined the role of cDC1s and B cells in guiding the differentiation of Th1 and Tfh cells from the
318 Th1/Tfh precursor. The role of cDC1s was determined by using *Batf3*$^{-/-}$ mice on a C57BL6/J background
319 (Edelson et al., 2010, 2011; Hildner et al., 2008), which display complete loss of migratory cDC1s (MHCII^{hi}
320 CD11c^{int} CD103$^+$ XCR1$^+$) and partial loss of resident cDC1s (MHCII^{int} CD11c^{hi} XCR1$^+$) (**Supplementary Figure**
321 **7A-F**). The role of B cells was determined by effective B-cell depletion using a mAb to CD20 prior to vaccination
322 (**Supplementary Figure 7G**). In both experimental set-ups, OTII cells were adoptively transferred, the MHC-
323 II:OVA vaccine was administered, and responses were read out in the dLNs by flow cytometry at day 5 after
324 vaccination. Neither *Batf3*-deficiency (**Supplementary Figure 7H, I**), nor B cell depletion (**Supplementary**
325 **Figure 7L, M**) affected the clonal expansion of endogenous PADRE tet$^+$ CD4 T cells or OTII cells. Formation of

326 CD44^{+} CXCR3^{+} CXCR5^{+} Th1/Tfh precursor cells was also unaffected in mice lacking these APCs (**Figure 6A,**
327 **B**). However, *Batf3*$^{-/-}$ mice showed a decrease in the generation of Th1, but not Tfh cells, while B-cell depleted
328 mice showed a decrease in the generation of Tfh, but not Th1 cells. This was the case for both endogenous
329 PADRE tet^{+} CD4 T cells (**Figure 6C-F**) and for exogenous OTII cells (**Supplementary Figure 7J-K, N-O**).
330 Altogether, these data suggest that CD28-dependent formation of the Th1/Tfh precursor pool is instructed by
331 APCs other than cDC1s and B cells, most likely cDC2s. Thereafter, in a second step of priming, the precursor
332 cells are instructed for Th1 differentiation on cDC1 as driven by CD40 costimulation, or for Tfh differentiation on
333 B cells, as driven by ICOS costimulation (**Figure 6G**).

334

335 ## Discussion

336 In this study, we show that upon *in vivo* activation, individual clones within the endogenous CD4 T-cell repertoire
337 transit through a bipotent Th1/Tfh precursor state before committing to Th1 or Tfh cell differentiation. These
338 precursor cells are in an early stem-like differentiation state characterized by TCF1 and SLAMF6, and they co-
339 express Th1- and Tfh-related markers at mRNA and protein level. Th1/Tfh precursor cells retain the capacity to
340 differentiate into both Th1 and Tfh cells, with TCR sharing underscoring their common origin. They arise
341 following vaccination as well as acute or chronic LCMV infection. Th1/Tfh precursor cells resemble, but are
342 distinct from, previously described memory-precursor populations, which are specifically enriched upon chronic
343 LCMV infection (Xia et al., 2022). Instead, they align with a previous study identifying a common Th1/Tfh
344 precursor among *Plasmodium chabaudi*-specific TCR transgenic CD4 T cells (Lönnberg et al., 2017). Together,
345 these findings establish the Th1/Tfh precursor state as a common feature in the CD4 T-cell differentiation
346 trajectory in type 1 immunity.

347 During priming in secondary lymphoid organs, T cells have multiple contacts with different APCs. This
348 is most explicit for Tfh formation in which both cDCs and B cells play a role. CD4 T cells are generally primed
349 by cDC2s in the T-cell zone (Gerner et al., 2017; Krishnaswamy et al., 2017; Li et al., 2016), giving rise to
350 CXCR5-expressing cells that are generally referred to as pre-Tfh cells. These cells migrate along a CXCL13
351 gradient from the T-cell zone towards the border of the B-cell follicle or the interfollicular region (IFR) (Crotty,
352 2014; Kerfoot et al., 2011). At that location, they receive further stimulation to enter the B-cell follicle and
353 complete Tfh differentiation (Kerfoot et al., 2011; Kim et al., 2024; Song & Craft, 2024). Although expression of
354 CXCR5 and PD-1 on activated CD4 T cells early after vaccination is generally considered indicative of Tfh
355 commitment, not all CXCR5$^+$ PD-1$^+$ CD4 T cells become Tfh cells (Kerfoot et al., 2011; Song & Craft, 2024).
356 This can now be explained by our definition of the CXCR3$^+$ CXCR5$^+$ Th1/Tfh precursor state. Thus far, CXCR3
357 that binds IFN-responsive chemokines CXCL9 and CXCL10, is generally associated with Th1 differentiation
358 (Groom et al., 2012). This chemokine receptor promotes migration of activated CD4 T cells from the T-cell zone
359 towards the IFR of the LN (Groom et al., 2012). Here, CD4 T-cell help for CD8 effector and memory
360 differentiation is likely delivered upon cognate contact of both CD4 and CD8 T cells with the same cDC1
361 (Duckworth et al., 2021; Eickhoff et al., 2015; Hor et al., 2015). However, activated CD4 T cells can also interact
362 with B cells in the IFR (Kerfoot et al., 2011). In line with the existence of the Th1/Tfh precursor, CXCR3 has
363 previously been found on cells with a Tfh phenotype (Künzli & Masopust, 2023; Weinstein et al., 2018). We

364 show that CXCR3$^+$ CXCR5$^+$ cells are bipotent Th1/Tfh precursors and propose that they correspond to
365 previously defined pre-Tfh cells. We postulate that the differentiation fate of these cells depends on the
366 dominance of either of the chemokine cues, allowing CXCR5-mediated guidance to a B cell for Tfh differentiation
367 or CXCR3-mediated guidance to a cDC1 for Th1 differentiation.

368 Accordingly, we found that cDC1 and CD40:CD40L interaction are required for Th1 differentiation from
369 the common precursor and B cells and ICOS costimulation are required for Tfh differentiation. CD40 signaling
370 in cDC1 is associated with upregulation of costimulatory molecules such as CD70, expression of IL-12 and
371 apoptosis resistance (Lei et al., 2024; Schulz et al., 2000; Wu et al., 2022). CD40 is also critical in the
372 maintenance of Tfh and GC responses (Baumjohann et al., 2013), and it was somewhat surprising that blockade
373 did not affect Tfh cell differentiation in our model. Similarly, CD86 is known to promote Tfh differentiation (Wang
374 et al., 2015), but we did not find any effects of single CD86 blockade. This may be explained by the fact that we
375 focused on early differentiation stages, prior to the establishment of germinal centers, when CD40 and CD86
376 signals may be trivial or compensated for. In addition to cDC1, CD40 signals and CXCR3-attracting chemokines
377 can also be delivered by monocyte-derived (Mo)DCs present within the IFR (Duckworth et al., 2021). This aligns
378 with our recent data showing that CD4 T cells and MoDCs communicate in a CD40-dependent feed-forward
379 loop to enforce Th1 effector differentiation (Bosma et al., 2025), which can be mediated by IL-12 (De Koker et
380 al., 2017; Leal et al., 2021).

381 The formation of the bipotent Th1/Tfh state allows immune system flexibility in tailoring host protection
382 to ongoing infections. Different viral infections can result in different Th1/Tfh ratios, which are reinforced through
383 regulatory feedback loops that suppress the expression of T-bet or BCL6 (J. Choi et al., 2020; De Giovanni et
384 al., 2020; Duckworth & Groom, 2021; Sheikh & Groom, 2021). Indeed, LCMV-Armstrong and Influenza infection
385 differentially depend on T-bet expression (Sheikh & Groom, 2021). Similarly, vesicular stomatitis virus (VSV)
386 induces a higher Tfh/Th1 ratio than LCMV by inducing an early wave of IFN-I and IL-6 (De Giovanni et al.,
387 2020). Thus, the formation of Th1/Tfh precursors and their subsequent differentiation will be context dependent.
388 Overcoming a certain threshold of T-bet versus BCL6 expression is likely essential to consolidate Th1 or Tfh
389 differentiation (Oestreich et al., 2012).

390 In human peripheral blood, CXCR3$^+$ CXCR5$^+$ PD-1^{lo} cells have been found, as well as Tfh-like cells that
391 share chemokine receptor and transcription factor expression with Th2 or Th17 cells (Morita et al., 2011).
392 CXCR3$^+$ Tfh-like cells have been associated with improved responses to influenza vaccination and correlate
393 with neutralizing antibodies in HIV controllers (Bentebibel et al., 2013, 2016; Martin-Gayo et al., 2017). These

394 circulating Tfh-like cells express CD62L and CCR7, suggesting that they are in a less differentiated or memory-
395 like state (Morita et al., 2011) and remain responsive to antigenic stimulation. Possibly, these cells represent
396 the Th1/Tfh precursors we have identified here.

397 The stem-like CD4 T cells that have been identified in transplantation rejection and cancer, and precede
398 Th1 differentiation (Cardenas et al., 2024; Zou et al., 2024), may also represent Th1/Tfh precursors. In
399 transplantation models, these stem-like CD4 T cells relied on metabolic rewiring, including *Ldha* expression
400 (Zou et al., 2024), which was also upregulated in Th1/Tfh precursors following vaccination. In cancer models,
401 they differentiated into Th1 cells upon Treg depletion (Cardenas et al., 2024). These stem-like CD4 T cells have
402 primarily been characterized using markers that are established for CD8 T cells. Many of these markers,
403 including TCF1, PD-1 and SLAMF6, are also expressed by the common Th1/Tfh precursor, supporting the
404 general concept of a stem-like, highly proliferative and uncommitted cell state. A recent pan-cancer analysis
405 across 21 tumor types further supports this concept, identifying a tumor-enriched CD4 T-cell population
406 predicted to be tumor-specific and characterized by both Th1- and Tfh-associated gene expression (Zheng et
407 al., 2021). Together, these findings underscore the need to generally acknowledge the Th1/Tfh precursor cell
408 state and to fully define the developmental cues for either Th1 or Tfh differentiation from this state.

409 ## Materials and Methods

410

411 **Mice**

412 Mice were housed in individually ventilated cages (IVC) under specific pathogen free (SPF) conditions and with
413 *ad libitum* access to food and water. Ambient temperature was ~19-21°C and humidity 30-70%. Lighting was
414 provided on a 12 h light/dark cycle. Eight-week-old male and female C57BL/6JRj mice were purchased from
415 Janvier laboratories (Le Genest Saint Isle, France). OTII*CD45.1 ((TcraTcrb)425Cbn/CrlLumc) on a C57BL/6JRj
416 background were bred in house. Batf3$^{-/-}$ (B6.129S(C)-Batf3tm1Kmm/J) on a C57BL/6J background and wild
417 type controls were obtained from The Jackson Laboratory. All mouse experiments were performed in
418 accordance with institutional and national guidelines and were approved by the Animal Welfare Body at Leiden
419 University Medical Center.

420

421 **DNA tattoo vaccination**

422 The cDNAs encoding the MHC-II, MHC-II:OVA and control sequences used for DNA vaccination were
423 expressed in a pVAX1 plasmid vector. MHC-II and control vaccines have previously been described (Ahrends
424 et al., 2016; Oosterhuis et al., 2012). MHC-II:OVA and MHC-II-GP(61-80) vaccines were generated by excising
425 the cassette encoding the MHC-II epitopes (p30, PADRE, HIV Nef$_{56-68}$) from the MHC-II vaccine cDNA with
426 HindIII and XhoI restriction enzymes, and replacing it with a gBlock containing the MHC-II cassette linked to
427 nucleotide sequences encoding OVA$_{323-339}$ (ISQAVHAAHAEINEAGR) or LCMV-Armstrong derived GP$_{61-80}$
428 (GLKGPDIYKGVYQFKSVEFD) and a GPGPGPG linker on both ends as for the original MHC-II vaccine.

429 For intraepidermal DNA tattoo vaccination (Ahrends et al., 2016; Babała et al., 2018), mice were anesthetized
430 using isoflurane (induction phase: 4% isoflurane, airflow 0.8 l/min; maintenance phase: 2% isoflurane, airflow
431 0.4 l/min) and the right hind leg of mice was depilated using Veet containing limonene (Reckitt Benckiser).
432 Subsequently, 15 ml of a 2 mg/ml plasmid DNA in H_2O was tattooed into the skin with a Permanent Make Up
433 tattoo machine (Cheyenne, MT Derm GmbH) using a sterile disposable needle with a needle depth of 1 mm.
434 Tattooing was performed for 45 sec, oscillating at a frequency of 100 Hertz. Mice were vaccinated at days 0, 3,
435 and 6 unless otherwise indicated, and alternating between the internal or external upper part of the right hind
436 leg.

437 **Adoptive T-cell transfer**

438 For adoptive transfer, spleens were isolated from 8- to 12-week-old, sex matched OTII*CD45.1 mice after
439 euthanasia. Spleens were mechanically disrupted and passed through a 70 mM Falcon strainer (Corning).
440 Subsequently, single cell suspensions were incubated in red blood cell (RBC) lysis buffer (Santa Cruz) for 5 min
441 at room temperature. CD4 T cells were isolated by negative selection using a CD4 T-cell isolation kit (Miltenyi)
442 according to the manufacturer's protocol. If indicated, purified OTII*CD45.1 CD4 T cells were labelled with 2.5
443 mM CFSE (Invitrogen) for 10 min at 37°C. Free CFSE was then quenched by adding at least five times excess
444 of Iscove's modified Dulbecco's medium (IMDM) with L-glutamine (Capricorn) and 10% fetal bovine serum
445 (FBS), 100 units/ml penicillin and 100 mg/ml streptomycin (Gibco), and resting cells for 5 min at room
446 temperature. Cell purity (>90%) and CFSE-labelling were checked for each experiment by flow cytometry using
447 the following monoclonal antibodies (mAbs) against mouse molecules: 1:100 CD45.1 BUV395 (clone A20, BD
448 Biosciences), 1:200 CD4 BUV805 (clone GK1.5, BD Biosciences), 1:200 TCRva2 BV421 (clone
449 B20.1),TCRvb5.1/5.2 (clone MR9-4), 1:100 CD44 BV570 (clone IM7), and 1:100 CD62L PE-Fire 810 (clone
450 W18021D; all BioLegend). C57BL/6JRj mice received 0.1 x 10^6 or 0.5 x 10^6 or 1 x 10^6 OTII*CD45.1 cells in 100
451 µl Hank's Balanced Salt Solution (HBSS) depending on the day of read out, or 5 x 10^5 purified SMARTA*GFP
452 (B6.Cg-Ptprca Pepcb Tg(TcrLCMV)1Aox/PpmJx) cells in 100 µl HBSS, kindly provided by Dr. K. Jobin and Prof.
453 W. Kastenmüller (University of Würzburg, Germany), by retro-orbital i.v. injection.

454

455 **Antibody and reagent treatment of mice**

456 All antibodies or reagents were injected intraperitoneally (i.p.). Mice received 250 mg depleting anti-CD20 mAb
457 (MB20-11, BioXcell) at day -2. Mice with incomplete B-cell depletion were excluded from analysis. For blocking
458 costimulatory ligands, mice received injections on days 0 and 3 post vaccination with 150 mg anti-CD40L mAb
459 (MR-1, BioXcell), 200 mg anti-CD80 mAb (1G10, BioXcell), 200 mg anti-CD86 mAb (GL-1, BioXcell) or 200 mg
460 anti-ICOSL mAb (HK5.3). FTY720 (Fingolimod, Cayman Chemicals) was dissolved in 96% ethanol at 20 mg/ml
461 and prior to injection diluted in 0.9% NaCl. Mice received 25 mg FTY720 in 200 ml 0.9% NaCl at days 0, 3 and
462 6.

463

464 **Cell isolation**

465 On the day of readout, mice were euthanized and organs collected. Blood was collected by tail vein puncture
466 or cardiac puncture. Erythrocytes were lysed by incubation in RBC lysis buffer (Santa Cruz) for 5 min at room
467 temperature. Inguinal dLNs of the vaccination site were punched repeatedly with a 25G needle and incubated
468 for 30 min at 37°C while shaking in 100 mg/ml Liberase TL (Roche) prepared in 500 ml DMEM. Enzymatic
469 digestion was quenched by adding FBS-supplemented IMDM, and single cell suspensions prepared by
470 mechanical disruption of dLNs through 70 mm Falcon strainers (Corning).

471

472 **Flow cytometry**

473 For cell surface staining, mAbs were diluted in FACS buffer (PBS + 2% FBS). Single cell suspensions were first
474 incubated for 1 h at room temperature with 1:200 PE-conjugated PADRE tetramer (AKFVAAWTLKAA in I-A(b),
475 NIH tetramer facility), and then for 30 min on ice with the following mAbs: 1:200 CD4 BUV805 (clone GK1.5),
476 1:200 PSGL1 BUV661 (clone 2PH1), 1:200 CD8a BV750 (clone 53-6.7), 1:00 CD8a V500 (clone 53-6.7), 1:400
477 CD95 BV605 (clone Jo2), 1:100 CD45.1 BUV395 (clone A20, all BD Biosciences), 1:200 CD138 (clone 281-2),
478 1:400 GL7 FITC (clone GL-7), 1:600 IgD PerCP-Cy5.5 (clone 11-26c2a), 1:100 CD44 BV570 (clone IM7), 1:100
479 CD44 BV785 (clone IM7), 1:100 CD62L PE-Fire 810 (clone W18021D), 1:100 PD-1 APC-Fire 810 (29F.1A12),
480 1:100 SLAM BV785 (clone TC15-12F12.2), 1:100 SLAMF6 Pacific Blue (clone 330-AJ), 1:100 CD3 PE-Fire 700
481 (17A2), 1:50 CXCR5 BV711 (clone L138D7), 1:50 CXCR3 BV605 (clone CXCR3-173, all BioLegend), 1:200
482 TACI APC (clone ebio8F10-3, eBioscience), 1:800 CD19 BUV661 (clone ebio1D3, Invitrogen) and APC-
483 conjugated E7 tetramer (E7(49-57) RAHYNIVTF in H-2D^{b}, produced in house). Dead cells were excluded using
484 1:500 Zombie UV fixable viability dye (BioLegend) or 1:1000 LIVE/DEAD NIR fixable viability dye (Invitrogen).

485 For intracellular staining of T cell-related markers, cells were fixed with the Foxp3/Transcription factor
486 staining kit (eBioscience). For intracellular staining of B cell-related markers, cells were fixed with BD
487 Cytofix/Cytoperm (BD Biosciences). In both cases, fixation was performed for 30 min on ice. After fixation, cells
488 were either permeabilized and intracellularly stained directly or washed with FACS buffer and frozen gradually
489 at -80°C in 10% DMSO and 90% FBS. Upon thawing, cells were washed with FACS buffer and re-fixed for 5
490 min at room temperature prior to permeabilization and intracellular antibody staining. The following mAbs were
491 used: 1:50 BCL6 BUV737 (clone K112-91), 1:50 GATA3 BUV395 (clone L50-823), 1:100 RORγt BV480 (clone
492 Q31-378, all BD Biosciences), 1:100 TCF1 Alexa fluor 488 (clone C63D9, Cell Signalling Technology), 1:200 T-
493 bet eFluor 660 (clone ebio4B10, eBioscience) and 1:100 FOXP3 PE-Cy5 (clone FJK16s, Invitrogen). Data were

494 acquired using a Cytek Aurora Spectral Flow Cytometer equipped with 355 nm, 405 nm, 488 nm, 561 nm and
495 640 nm lasers (Cytek Biosciences), and analysed with OMIQ (Dotmatics version 2024.07) or FlowJo software
496 (TreeStar, version 10.8.1).

497 UMAP analysis and Wishbone trajectory analysis were performed using OMIQ on a maximum of 1000
498 PADRE^{+} CD4^{+} T cells per mouse (N=5/time point, total 27867 cells). For dimension reduction and Wishbone
499 analysis, the following markers were included: PSGL1, FR4, BCL6, SLAMF6, CD44, CXCR5, SLAM, TCF1,
500 CD62L, T-bet and PD-1. For Wishbone analysis, diffusion maps were generated first and then Wishbone was
501 performed from diffusion components, with naïve (CD62L^{+} CD44^{-} PD-1^{-} SLAMF6^{-}) cells selected as starting
502 point.

503

504 **Preparations for transcriptome analysis**

505 Mice received MHC-II vaccine and cells were harvested at day 5 or 10 after the first vaccination. Single cell
506 suspensions of dLNs from 3 mice per time point were pooled to reduce biological variability. Samples were
507 incubated with 1:50 anti-mouse CD16/32 mAb (Fc Block™, clone 2.4G2, BD Biosciences) in BD Stain buffer
508 (with FBS, BD Biosciences) for 5 min on ice and subsequently stained with the following mAbs in BD stain
509 buffer: 1:100 CD3 BV421 (clone 17A2, Biolegend), 1:100 CD19 PerCP-Vio700 (clone REA749, Miltenyi
510 Biotech), 1:100 CD44 PE-Cy7 (clone IM7, eBioscience), 1:100 CD62L FITC (clone Mel-14, eBioscience) and
511 1:1000 LIVE/DEAD Fixable Near-IR dye (Invitrogen). CD3^{+} CD44^{hi} CD62L^{lo} cells were FACS-sorted on a
512 FACSAria II (BD Biosciences). Subsequently, samples were stained with unique hashtag oligonucleotide (HTO)-
513 conjugated antibodies to CD45/MHC-I (TotalSeq C hashtags, C0301 to C0307 and C0309, BioLegend). Staining
514 was performed according to the manufacturer's instructions. Briefly, FACS-sorted T cells were stained with 0.5
515 mg TotalSeq hashtag per sample for 30 min on ice and washed 5 times with PBS + 0.04% BSA. Prior to last
516 wash, cells were passed through a 40 mm Flowmi Cell Strainer (Sigma-Aldrich) and samples were pooled.
517 scRNAseq libraries were created according to the manufacturer's protocol, using a 10X Chromium single cell
518 5'v2 chemistry kit (10X Genomics). TCRseq was library was prepared using a 10X Chromium single cell V(D)J
519 enrichment kit for mouse T cells (10X Genomics). Nucleotide sequencing was performed on a NovaSeq6000
520 system (Illumina). In total, 25132 cells were analyzed for sequencing with a median sequencing-depth of 11196
521 reads per cell.

522

523 **Processing, integration and clustering of transcriptome data**

524 Analysis of scRNAseq and TCRseq data was performed using CellRanger (10X Genomics, v6.0.1) and Seurat
525 (v4.3.0) in R (v4.2.3). scRNAseq reads were aligned to the mouse reference genome mm10, and barcode
526 counting was performed using 'cellranger count'. TCRseq reads were aligned to the mouse reference genome
527 mm10 and consensus TCR sequences were determined using 'cellranger vdj'. From the gene expression count
528 matrix, TCR and BCR genes were removed using the 'grep' function in R with the patterns "^Tr[abgd][cvdj]" and
529 "Ig[hkl][cvdj]" respectively. After this, the dataset was analyzed in R using the standard Seurat pipeline. Seurat
530 object was created using 'CreateSeuratObject,' with a minimum of 200 features per cell and 3 cells expressing
531 each gene. HTO sequencing data was added as a separate assay to the Seurat object using
532 'CreateAssayObject' and HTO counts were normalized by CLR method using 'NormalizeData.' HTO
533 demultiplexing was performed using 'HTODemux' with a positive quantile of 0.99. As a result of this, each cell
534 in the dataset was assigned to a global (singlet, doublet, or negative) and a sample-related HTO classification.
535 Heatmap was created of HTO demultiplexing result using 'HTOHeatmap.' Singlets were selected using 'subset',
536 and gene expression data was normalized using 'NormalizeData'. Variable features were determined using
537 'FindVariableFeaures' with the selection method 'mean.var.plot'. Data was scaled using 'ScaleData' on variable
538 features. Percentage of mitochondrial gene expression per cell was determined using 'PercentageFeatureSet'
539 with the pattern "^mt-". Singlets were filtered on number of RNA features (between 400 and 5000), number of
540 RNA counts (<25000) and mitochondrial gene expression (<10%). Cell cycle scores for G2/M and S phase were
541 assigned using 'CellCycleScoring', based on expression of G2/M and S phase genes. Data was normalized
542 using 'NormalizeData' with normalization method 'LogNormalize', scale factor 25000. Top 2000 variable features
543 were determined using 'FindVariableFeatures' with the selection method 'vst'. Data was scaled using
544 'ScaleData', whereby G2M scores, S scores and percentage of mitochondrial gene expression were regressed
545 out. Principle component analysis (PCA) was run using 'RunPCA' on variable features. Clustering was
546 performed on first 20 principal components (PCs) using 'FindNeighbors' and 'FindClusters'. Clustering
547 resolution was set to 0.5. Uniform manifold approximation and projection (UMAP) visualization was performed
548 using 'RunUMAP' on the first 20 PCs. Expression of known marker genes was visualized per cluster and within
549 the UMAP projection using 'Dotplot', 'VlnPlot' and 'FeaturePlot' functions. Clusters with contaminating B cells
550 (expression of *Cd19*, *Ms4a1*), APCs (expression of *Cd40*, *Cd274*, *Cd80*, *Cd86*) and low-quality cells (high
551 percentage mitochondrial genes, low RNA counts) were removed. The pipeline was run again on filtered T cells,
552 including determining variable features, data scaling, PCA, clustering and UMAP visualization. CD4 T-cell

553 clusters were selected by expression of *Cd4*, in absence of expression of *Cd8a* and *Cd8b1* or TCRg/d. Within
554 CD4 T-cell subsets, Help d5 and Help d10 were selected for further analysis. Clusters were annotated based
555 on differentially expressed genes. Venn Diagrams were created with
556 http://bioinformatics.psb.ugent.be/webtools/Venn/.

557 Previously generated scRNAseq datasets from I-A^b-LCMV-gp66 tetramer-sorted CD4 T cells from
558 LCMV-Armstrong or LCMV-Clone 13 derived at day 8 and day 21 post infection were obtained from (Xia et al.,
559 2022). Feature barcode matrices derived from 10x scRNA expression libraries reads aligned to mouse genome
560 assembly GRCm38 were imported into R (version 4.4.0). A Seurat-based (version 5.2.1) quality control on the
561 scRNA-seq samples was performed individually. TCR and BCR counts were removed from the raw gene
562 expression count matrix (UMI) to prevent TCR/BCR chain driven clustering bias. A per-sample Seurat object
563 was created by selecting cells on the criterium of containing a minimum of 200 genes and genes on being
564 expressed in a minimum of 3 cells. Cells (~30%) were excluded from the subsequent analysis based on the
565 mitochondrial content (>5%), RNA count (<1000 and >25000) and genetic content (<400 and >4000) The top
566 2000 highly variable genes were selected using 'FindVariableFeatures' for subsequent analysis. Cells of all 19
567 samples were normalized and scaled individually while regressing out mitochondrial gene expression and cell
568 cycle scores for G2/M and S phase genes assigned using 'CellCycleScoring' as described above. Clustering
569 was done on the first 30 principal components (PCs) with the default cluster resolution. Doublets were removed
570 using 'DoubletFinder' based on the first 40 principal components (PCs).

571 Singlets of each sample were integrated by identifying anchors between datasets, using the top 2000
572 variable genes, 30 reciprocal PCA dimensions and an integration strength of 5. Clusters with contaminating B
573 cells (expression of Cd19 Ms4a1), CD8 T cells (expression of Cd8a, Cd8b), APCs (expression of Cd40, Cd80,
574 Cd86) or low-quality cells were removed. Data scaling and PCA was done once more on the integrated and
575 filtered object. A k-nearest neighbors graph was generated with the first 20 PCs and community detection for
576 cluster identification was performed using the Louvain algorithm with a resolution of 0.4. The integrated matrix
577 visualized as an UMAP was subsequently divided based on the day of infection (Day 8 or Day 21) and the viral
578 strain (LCMV-Arm and LCMV-c13) as annotated in the metadata of the Seurat object.

579 Clusters were annotated based on differentially expressed genes. Subsequently, clusters were
580 compared to CD4 T cell-specific signatures derived from Th1, Tfh or Th1/Tfh precursors, all derived from vaccine
581 induced CD4 T cells from this article, or to a curated stem-like signature (Cardenas et al., 2024) to enable cluster

annotation via scoring based on gene signature module scores, which were calculated using Seurat's 'AddModuleScore' function by averaging the expression of the signature genes for each cell. cluster defining markers were selected and the relative normalized expression values represented in z-scores were visualized in a heatmap using Seurat's 'pheatmap'.

Statistics

For mouse experiments, statistical analysis was performed with GraphPad Prism 9.3.1 (Dotmatics) using two-tailed unpaired Student *t*-test when comparing two groups, One-Way ANOVA with Dunnett post hoc test to correct for multiple testing when comparing multiple groups at one timepoint or Two-Way ANOVA with Šidák post hoc test to correct for multiple testing when comparing multiple groups at multiple time points. P values < 0.05 were considered statistically significant. Statistics were denoted as follows; *; P≤0.05, **; P≤0.01, ***; P≤0.001 and ****; P≤0.0001. Plots were generated with ggplot2 (3.3.3) and GraphPad Prism 9.3.1.

Author contributions

Conceptualization: D.M.T.B, J.Bo, F.S. Methodology and investigation: D.M.T.B, J.Bu, M.D.S, X.L, T.d.W, Y.X, F.S. Formal analysis, visualization and data curation: D.M.T.B, J.Bu, M.d.K, F.S. Writing - original draft: D.M.T.B, J.Bo, F.S. Writing - review and editing: D.M.T.B, J.Bu, M.D.S, M.d.K, X.L, T.d.W, Y.X, J.Bo, F.S. Project administration, funding acquisition and supervision: J.Bo. and F.S.

Acknowledgements

We thank the Animal facility, Flow Cytometry Facility and Leiden Genome Technology Center from the LUMC for technical assistance. This work was supported by grants 11079 (to J.B. and Y.X) and 10894 (to J.B.) from the Dutch Cancer Society (KWF); a grant from Oncode to JB, and a VENI grant (ZonMw project n. 09150162010046) from the Dutch Science Foundation (NWO) to F.S.

Declaration of interests

The authors declare no competing interests.

Supplemental information

- Document S1: Supplementary figures 1-7.

References

Agata, Y., Kawasaki, A., Nishimura, H., Ishida, Y., Tsubata, T., Yagita, H., & Honjo, T. (1996). Expression of the PD-1 antigen on the surface of stimulated mouse T and B lymphocytes. *International Immunology*, *8*(5), 765–772. https://doi.org/10.1093/INTIMM/8.5.765

Ahrends, T., Babała, N., Xiao, Y., Yagita, H., Van Eenennaam, H., & Borst, J. (2016). CD27 Agonism Plus PD-1 Blockade Recapitulates CD4 + T-cell Help in Therapeutic Anticancer Vaccination. *Cancer Research*, *76*(10), 2921–2931. https://doi.org/10.1158/0008-5472.CAN-15-3130

Ahrends, T., Busselaar, J., Severson, T. M., Bąbała, N., de Vries, E., Bovens, A., Wessels, L., van Leeuwen, F., & Borst, J. (2019). CD4+ T cell help creates memory CD8+ T cells with innate and help-independent recall capacities. *Nature Communications*, *10*(1). https://doi.org/10.1038/S41467-019-13438-1

Ahrends, T., Spanjaard, A., Pilzecker, B., Bąbała, N., Bovens, A., Xiao, Y., Jacobs, H., & Borst, J. (2017). CD4+ T Cell Help Confers a Cytotoxic T Cell Effector Program Including Coinhibitory Receptor Downregulation and Increased Tissue Invasiveness. *Immunity*, *47*(5), 848-861.e5. https://doi.org/10.1016/J.IMMUNI.2017.10.009

Alexander, J., Sidney, J., Southwood, S., Ruppert, J., Oseroff, C., Maewal, A., Snoke, K., Serra, H. M., Kubo, R. T., Sette, A., & Grey, H. M. (1994). Development of high potency universal DR-restricted helper epitopes by modification of high affinity DR-blocking peptides. *Immunity*, *1*(9), 751–761. https://doi.org/10.1016/S1074-7613(94)80017-0

Alterauge, D., Bagnoli, J. W., Dahlström, F., Bradford, B. M., Mabbott, N. A., Buch, T., Enard, W., & Baumjohann, D. (2020). Continued Bcl6 Expression Prevents the Transdifferentiation of Established Tfh Cells into Th1 Cells during Acute Viral Infection. *Cell Reports*, *33*(1), 108232. https://doi.org/10.1016/J.CELREP.2020.108232

Babała, N., Bovens, A., De Vries, E., Iglesias-Guimarais, V., Ahrends, T., Krummel, M. F., Borst, J., & Bins, A. D. (2018). Subcellular localization of antigen in keratinocytes dictates delivery of CD4 þ T-cell Help for the CTL response upon therapeutic DNA vaccination into the Skin. *Cancer Immunology Research*, *6*(7), 835–847. https://doi.org/10.1158/2326-6066.CIR-17-0408

Baumeister, S. H., Freeman, G. J., Dranoff, G., & Sharpe, A. H. (2016). Coinhibitory Pathways in Immunotherapy for Cancer. *Annual Review of Immunology*, *34*, 539–573. https://doi.org/10.1146/ANNUREV-IMMUNOL-032414-112049

Baumjohann, D., Okada, T., & Ansel, K. M. (2011). Cutting Edge: Distinct Waves of BCL6 Expression during T Follicular Helper Cell Development. *The Journal of Immunology*, *187*(5), 2089–2092. https://doi.org/10.4049/JIMMUNOL.1101393

Baumjohann, D., Preite, S., Reboldi, A., Ronchi, F., Ansel, K. M., Lanzavecchia, A., & Sallusto, F. (2013). Persistent Antigen and Germinal Center B Cells Sustain T Follicular Helper Cell Responses and Phenotype. *Immunity*, *38*(3), 596–605. https://doi.org/10.1016/J.IMMUNI.2012.11.020

Bentebibel, S. E., Khurana, S., Schmitt, N., Kurup, P., Mueller, C., Obermoser, G., Palucka, A. K., Albrecht, R. A., Garcia-Sastre, A., Golding, H., & Ueno, H. (2016). ICOS+PD-1+CXCR3+ T follicular helper cells contribute to the generation of high-avidity antibodies following influenza vaccination. *Scientific Reports 2016 6:1*, *6*(1), 1–8. https://doi.org/10.1038/srep26494

Bentebibel, S. E., Lopez, S., Obermoser, G., Schmitt, N., Mueller, C., Harrod, C., Flano, E., Mejias, A., Albrecht, R. A., Blankenship, D., Xu, H., Pascual, V., Banchereau, J., Garcia-Sastre, A., Palucka, A. K., Ramilo, O., & Ueno, H. (2013). Induction of ICOS+CXCR3+CXCR5+ T H cells

correlates with antibody responses to influenza vaccination. *Science Translational Medicine*, *5*(176). https://doi.org/10.1126/SCITRANSLMED.3005191/SUPPL_FILE/5-176RA32_SM.PDF

Bins, A. D., Jorritsma, A., Wolkers, M. C., Hung, C. F., Wu, T. C., Schumacher, T. N. M., & Haanen, J. B. A. G. (2005). A rapid and potent DNA vaccination strategy defined by in vivo monitoring of antigen expression. *Nature Medicine*, *11*(8), 899–904. https://doi.org/10.1038/NM1264

Borst, J., Ahrends, T., Bąbała, N., Melief, C. J. M., & Kastenmüller, W. (2018). CD4+ T cell help in cancer immunology and immunotherapy. In *Nature Reviews Immunology* (Vol. 18, Issue 10, pp. 635–647). Nature Publishing Group. https://doi.org/10.1038/s41577-018-0044-0

Bosma, D. M. T., Busselaar, J., Staal, M. D., Frijlink, E., Mack, M., Salerno, F., & Borst, J. (2025). CD4+ T-cell help delivery to monocyte-derived dendritic cells promotes effector differentiation of helper and cytotoxic T cells. *Immunology Letters*, *275*. https://doi.org/10.1016/J.IMLET.2025.107022

Busselaar, J., Tian, S., van Eenennaam, H., & Borst, J. (2020). Helpless Priming Sends CD8+ T Cells on the Road to Exhaustion. *Frontiers in Immunology*, *11*, 2637. https://doi.org/10.3389/fimmu.2020.592569

Cardenas, M. A., Prokhnevska, N., Sobierajska, E., Gregorova, P., Medina, C. B., Valanparambil, R. M., Greenwald, R., DelBalzo, L., Bilen, M. A., Joshi, S. S., Narayan, V. M., Master, V. A., Sanda, M. G., & Kissick, H. T. (2024). Differentiation fate of a stem-like CD4 T cell controls immunity to cancer. *Nature 2024 636:8041*, *636*(8041), 224–232. https://doi.org/10.1038/s41586-024-08076-7

Cho, Y. L., Flossdorf, M., Kretschmer, L., Höfer, T., Busch, D. H., & Buchholz, V. R. (2017). TCR Signal Quality Modulates Fate Decisions of Single CD4+ T Cells in a Probabilistic Manner. *Cell Reports*, *20*(4), 806–818. https://doi.org/10.1016/J.CELREP.2017.07.005

Choi, J., Diao, H., Faliti, C. E., Truong, J., Rossi, M., Bélanger, S., Yu, B., Goldrath, A. W., Pipkin, M. E., & Crotty, S. (2020). Bcl-6 is the nexus transcription factor of T follicular helper cells via repressor-of-repressor circuits. *Nature Immunology*, *21*(7), 777–789. https://doi.org/10.1038/S41590-020-0706-5

Choi, Y. S., Gullicksrud, J. A., Xing, S., Zeng, Z., Shan, Q., Li, F., Love, P. E., Peng, W., Xue, H. H., & Crotty, S. (2015). LEF-1 and TCF-1 orchestrate TFH differentiation by regulating differentiation circuits upstream of the transcriptional repressor Bcl6. *Nature Immunology 2015 16:9*, *16*(9), 980–990. https://doi.org/10.1038/ni.3226

Choi, Y. S., Kageyama, R., Eto, D., Escobar, T. C., Johnston, R. J., Monticelli, L., Lao, C., & Crotty, S. (2011). ICOS Receptor Instructs T Follicular Helper Cell versus Effector Cell Differentiation via Induction of the Transcriptional Repressor Bcl6. *Immunity*, *34*(6), 932–946. https://doi.org/10.1016/J.IMMUNI.2011.03.023

Cibrián, D., & Sánchez-Madrid, F. (2017). CD69: from activation marker to metabolic gatekeeper. *European Journal of Immunology*, *47*(6), 946–953. https://doi.org/10.1002/EJI.201646837

Collins, A. V., Brodie, D. W., Gilbert, R. J. C., Iaboni, A., Manso-Sancho, R., Walse, B., Stuart, D. I., Van Der Merwe, P. A., & Davis, S. J. (2002). The interaction properties of costimulatory molecules revisited. *Immunity*, *17*(2), 201–210. https://doi.org/10.1016/S1074-7613(02)00362-X

Crotty, S. (2014). T follicular helper cell differentiation, function, and roles in disease. *Immunity*, *41*(4), 529–542. https://doi.org/10.1016/J.IMMUNI.2014.10.004

De Giovanni, M., Cutillo, V., Giladi, A., Sala, E., Maganuco, C. G., Medaglia, C., Di Lucia, P., Bono, E., Cristofani, C., Consolo, E., Giustini, L., Fiore, A., Eickhoff, S., Kastenmüller, W., Amit, I., Kuka, M., & Iannacone, M. (2020). Spatiotemporal regulation of type I interferon expression determines the antiviral polarization of CD4+ T cells. *Nature Immunology*, *21*(3), 321–330. https://doi.org/10.1038/s41590-020-0596-6

De Koker, S., Van Hoecke, L., De Beuckelaer, A., Roose, K., Deswarte, K., Willart, M. A., Bogaert, P., Naessens, T., De Geest, B. G., Saelens, X., Lambrecht, B. N., & Grooten, J. (2017). Inflammatory monocytes regulate Th1 oriented immunity to CpG adjuvanted protein vaccines through production of IL-12. *Scientific Reports*, *7*(1). https://doi.org/10.1038/S41598-017-06236-6

Den Haan, J. M. M., Lehar, S. M., & Bevan, M. J. (2000). CD8(+) but not CD8(-) dendritic cells cross-prime cytotoxic T cells in vivo. *The Journal of Experimental Medicine*, *192*(12), 1685–1695. https://doi.org/10.1084/JEM.192.12.1685

Ditoro, D., Winstead, C., Pham, D., Witte, S., Andargachew, R., Singer, J. R., Wilson, C. G., Zindl, C. L., Luther, R. J., Silberger, D. J., Weaver, B., Kolawole, M., Martinez, R. J., Turner, H., Hatton, R. D., Moon, J., Way, S. S., Evavold, B. D., & Weaver, C. T. (2018). Differential IL-2 expression defines developmental fates of follicular versus nonfollicular helper T cells. *Science*, *361*(6407). https://doi.org/10.1126/SCIENCE.AAO2933

Duckworth, B. C., & Groom, J. R. (2021). Conversations that count: Cellular interactions that drive T cell fate. *Immunological Reviews*, *300*(1), 203–219. https://doi.org/10.1111/IMR.12945

Duckworth, B. C., Lafouresse, F., Wimmer, V. C., Broomfield, B. J., Dalit, L., Alexandre, Y. O., Sheikh, A. A., Qin, R. Z., Alvarado, C., Mielke, L. A., Pellegrini, M., Mueller, S. N., Boudier, T., Rogers, K. L., & Groom, J. R. (2021). Effector and stem-like memory cell fates are imprinted in distinct lymph node niches directed by CXCR3 ligands. *Nature Immunology*, *22*(4), 434–448. https://doi.org/10.1038/S41590-021-00878-5

Dudziak, D., Kamphorst, A. O., Heidkamp, G. F., Buchholz, V. R., Trumpfheller, C., Yamazaki, S., Cheong, C., Liu, K., Lee, H. W., Chae, G. P., Steinman, R. M., & Nussenzweig, M. C. (2007). Differential antigen processing by dendritic cell subsets in vivo. *Science*, *315*(5808), 107–111. https://doi.org/10.1126/SCIENCE.1136080/SUPPL_FILE/DUDZIAK.SOM.PDF

Edelson, B. T., Bradstreet, T. R., KC, W., Hildner, K., Herzog, J. W., Sim, J., Russell, J. H., Murphy, T. L., Unanue, E. R., & Murphy, K. M. (2011). Batf3-dependent CD11b(low/-) peripheral dendritic cells are GM-CSF-independent and are not required for Th cell priming after subcutaneous immunization. *PloS One*, *6*(10). https://doi.org/10.1371/JOURNAL.PONE.0025660

Edelson, B. T., Wumesh, K. C., Juang, R., Kohyama, M., Benoit, L. A., Klekotka, P. A., Moon, C., Albring, J. C., Ise, W., Michael, D. G., Bhattacharya, D., Stappenbeck, T. S., Holtzman, M. J., Sung, S. S. J., Murphy, T. L., Hildner, K., & Murphy, K. M. (2010). Peripheral CD103+ dendritic cells form a unified subset developmentally related to CD8alpha+ conventional dendritic cells. *The Journal of Experimental Medicine*, *207*(4), 823–836. https://doi.org/10.1084/JEM.20091627

Eickhoff, S., Brewitz, A., Gerner, M. Y., Klauschen, F., Komander, K., Hemmi, H., Garbi, N., Kaisho, T., Germain, R. N., & Kastenmüller, W. (2015). Robust Anti-viral Immunity Requires Multiple Distinct T Cell-Dendritic Cell Interactions. *Cell*, *162*(6), 1322–1337. https://doi.org/10.1016/J.CELL.2015.08.004

Eisenbarth, S. C., Baumjohann, D., Craft, J., Fazilleau, N., Ma, C. S., Tangye, S. G., Vinuesa, C. G., & Linterman, M. A. (2021). CD4+ T cells that help B cells - a proposal for uniform nomenclature. *Trends in Immunology*, *42*(8), 658–669. https://doi.org/10.1016/J.IT.2021.06.003

Fang, D., Cui, K., Mao, K., Hu, G., Li, R., Zheng, M., Riteau, N., Reiner, S. L., Sher, A., Zhao, K., & Zhu, J. (2018). Transient T-bet expression functionally specifies a distinct T follicular helper subset. *Journal of Experimental Medicine*, *215*(11), 2705–2714. https://doi.org/10.1084/JEM.20180927

Fazilleau, N., McHeyzer-Williams, L. J., Rosen, H., & McHeyzer-Williams, M. G. (2009). The function of follicular helper T cells is regulated by the strength of T cell antigen receptor binding. *Nature Immunology*, *10*(4), 375–384. https://doi.org/10.1038/NI.1704

Ferris, S. T., Durai, V., Wu, R., Theisen, D. J., Ward, J. P., Bern, M. D., Davidson, J. T., Bagadia, P., Liu, T., Briseño, C. G., Li, L., Gillanders, W. E., Wu, G. F., Yokoyama, W. M., Murphy, T. L., Schreiber, R. D., & Murphy, K. M. (2020). cDC1 prime and are licensed by CD4+ T cells to induce anti-tumour immunity. *Nature*, *584*(7822), 624–629. https://doi.org/10.1038/S41586-020-2611-3

Gerner, M. Y., Casey, K. A., Kastenmuller, W., & Germain, R. N. (2017). Dendritic cell and antigen dispersal landscapes regulate T cell immunity. *The Journal of Experimental Medicine*, *214*(10), 3105–3122. https://doi.org/10.1084/JEM.20170335

Grewal, I. S., Xu, J., & Flavell, R. A. (1995). Impairment of antigen-specific T-cell priming in mice lacking CD40 ligand. *Nature*, *378*(6557), 617–620. https://doi.org/10.1038/378617A0

Groom, J. R., Richmond, J., Murooka, T. T., Sorensen, E. W., Sung, J. H., Bankert, K., von Andrian, U. H., Moon, J. J., Mempel, T. R., & Luster, A. D. (2012). CXCR3 chemokine receptor-ligand interactions in the lymph node optimize CD4+ T helper 1 cell differentiation. *Immunity*, *37*(6), 1091–1103. https://doi.org/10.1016/J.IMMUNI.2012.08.016

Hildner, K., Edelson, B. T., Purtha, W. E., Diamond, M., Matsushita, H., Kohyama, M., Calderon, B., Schraml, B. U., Unanue, E. R., Diamond, M. S., Schreiber, R. D., Murphy, T. L., & Murphy, K. M. (2008). Batf3 deficiency reveals a critical role for CD8alpha+ dendritic cells in cytotoxic T cell immunity. *Science (New York, N.Y.)*, *322*(5904), 1097–1100. https://doi.org/10.1126/SCIENCE.1164206

Hilligan, K. L., & Ronchese, F. (2020). Antigen presentation by dendritic cells and their instruction of CD4+ T helper cell responses. *Cellular & Molecular Immunology 2020 17:6*, *17*(6), 587–599. https://doi.org/10.1038/s41423-020-0465-0

Hor, J. L., Whitney, P. G., Zaid, A., Brooks, A. G., Heath, W. R., & Mueller, S. N. (2015). Spatiotemporally Distinct Interactions with Dendritic Cell Subsets Facilitates CD4+ and CD8+ T Cell Activation to Localized Viral Infection. *Immunity*, *43*(3), 554–565. https://doi.org/10.1016/J.IMMUNI.2015.07.020

Kageyama, R., Cannons, J. L., Zhao, F., Yusuf, I., Lao, C., Locci, M., Schwartzberg, P. L., & Crotty, S. (2012). The receptor Ly108 functions as a SAP adaptor-dependent on-off switch for T cell help to B cells and NKT cell development. *Immunity*, *36*(6), 986–1002. https://doi.org/10.1016/J.IMMUNI.2012.05.016

Kerfoot, S. M., Yaari, G., Patel, J. R., Johnson, K. L., Gonzalez, D. G., Kleinstein, S. H., & Haberman, A. M. (2011). Germinal center B cell and T follicular helper cell development initiates in the interfollicular zone. *Immunity*, *34*(6), 947–960. https://doi.org/10.1016/J.IMMUNI.2011.03.024

Kim, Y. J., Choi, J., & Choi, Y. S. (2024). Transcriptional regulation of Tfh dynamics and the formation of immunological synapses. *Experimental & Molecular Medicine 2024 56:6*, *56*(6), 1365–1372. https://doi.org/10.1038/s12276-024-01254-7

Kiner, E., Willie, E., Vijaykumar, B., Chowdhary, K., Schmutz, H., Chandler, J., Schnell, A., Thakore, P. I., LeGros, G., Mostafavi, S., Mathis, D., Benoist, C., Aguilar, O., Allan, R., Astarita, J., Austen, K. F., Barrett, N., Baysoy, A., Benoist, C., … Yoshida, H. (2021). Gut CD4+ T cell phenotypes are a continuum molded by microbes, not by TH archetypes. *Nature Immunology*, *22*(2), 216–228. https://doi.org/10.1038/S41590-020-00836-7

Krishnaswamy, J. K., Gowthaman, U., Zhang, B., Mattsson, J., Szeponik, L., Liu, D., Wu, R., White, T., Calabro, S., Xu, L., Collet, M. A., Yurieva, M., Alsén, S., Fogelstrand, P., Walter, A., Heath, W. R., Mueller, S. N., Yrlid, U., Williams, A., & Eisenbarth, S. C. (2017). Migratory CD11b+ conventional dendritic cells induce T follicular helper cell-dependent antibody responses. *Science Immunology*, *2*(18). https://doi.org/10.1126/SCIIMMUNOL.AAM9169

Künzli, M., & Masopust, D. (2023). CD4+ T cell memory. *Nature Immunology 2023*, *24*, 1–12. https://doi.org/10.1038/s41590-023-01510-4

Künzli, M., Reuther, P., Pinschewer, D. D., & King, C. G. (2021). Opposing effects of T cell receptor signal strength on CD4 T cells responding to acute versus chronic viral infection. *ELife*, *10*. https://doi.org/10.7554/ELIFE.61869

Künzli, M., Schreiner, D., Pereboom, T. C., Swarnalekha, N., Litzler, L. C., Lötscher, J., Ertuna, Y. I., Roux, J., Geier, F., Jakob, R. P., Maier, T., Hess, C., Taylor, J. J., & King, C. G. (2020). Long-lived T follicular helper cells retain plasticity and help sustain humoral immunity. *Science Immunology*, *5*(45). https://doi.org/10.1126/SCIIMMUNOL.AAY5552

Leal, J. M., Huang, J. Y., Kohli, K., Stoltzfus, C., Lyons-Cohen, M. R., Olin, B. E., Gale, M., & Gerner, M. Y. (2021). Innate cell microenvironments in lymph nodes shape the generation of T cell responses during type I inflammation. *Science Immunology*, *6*(56), eabb9435. https://doi.org/10.1126/sciimmunol.abb9435

Lei, X., de Groot, D. C., Welters, M. J. P., de Wit, T., Schrama, E., van Eenennaam, H., Santegoets, S. J., Oosenbrug, T., van der Veen, A., Vos, J. L., Zuur, C. L., de Miranda, N. F. C. C., Jacobs, H., van der Burg, S. H., Borst, J., & Xiao, Y. (2024). CD4+ T cells produce IFN-I to license cDC1s for induction of cytotoxic T-cell activity in human tumors. *Cellular & Molecular Immunology*, *21*(4), 374–392. https://doi.org/10.1038/S41423-024-01133-1

Li, J., Lu, E., Yi, T., & Cyster, J. G. (2016). EBI2 augments Tfh cell fate by promoting interaction with IL-2-quenching dendritic cells. *Nature 2016 533:7601*, *533*(7601), 110–114. https://doi.org/10.1038/nature17947

Linterman, M. A., Denton, A. E., Divekar, D. P., Zvetkova, I., Kane, L., Ferreira, C., Veldhoen, M., Clare, S., Dougan, G., Espéli, M., & Smith, K. G. C. (2014). CD28 expression is required after T cell priming for helper T cell responses and protective immunity to infection. *ELife*, *3*(October2014), 1–21. https://doi.org/10.7554/ELIFE.03180

Liu, D., Xu, H., Shih, C., Wan, Z., Ma, X., Ma, W., Luo, D., & Qi, H. (2014). T–B-cell entanglement and ICOSL-driven feed-forward regulation of germinal centre reaction. *Nature 2014 517:7533*, *517*(7533), 214–218. https://doi.org/10.1038/nature13803

Lönnberg, T., Svensson, V., James, K. R., Fernandez-Ruiz, D., Sebina, I., Montandon, R., Soon, M. S. F., Fogg, L. G., Nair, A. S., Liligeto, U. N., Stubbington, M. J. T., Ly, L. H., Bagger, F. O., Zwiessele, M., Lawrence, N. D., Souza-Fonseca-Guimaraes, F., Bunn, P. T., Engwerda, C. R.,

Heath, W. R., … Teichmann, S. A. (2017). Single-cell RNA-seq and computational analysis using temporal mixture modelling resolves Th1/Tfh fate bifurcation in malaria. *Science Immunology*, *2*(9). https://doi.org/10.1126/SCIIMMUNOL.AAL2192

Ma, C. S., Deenick, E. K., Batten, M., & Tangye, S. G. (2012). The origins, function, and regulation of T follicular helper cells. *The Journal of Experimental Medicine*, *209*(7), 1241. https://doi.org/10.1084/JEM.20120994

Marshall, H. D., Chandele, A., Jung, Y. W., Meng, H., Poholek, A. C., Parish, I. A., Rutishauser, R., Cui, W., Kleinstein, S. H., Craft, J., & Kaech, S. M. (2011). Differential Expression of Ly6C and T-bet Distinguish Effector and Memory Th1 CD4+ Cell Properties during Viral Infection. *Immunity*, *35*(4), 633–646. https://doi.org/10.1016/J.IMMUNI.2011.08.016

Martínez-López, M., Iborra, S., Conde-Garrosa, R., & Sancho, D. (2015). Batf3-dependent CD103+ dendritic cells are major producers of IL-12 that drive local Th1 immunity against Leishmania major infection in mice. *European Journal of Immunology*, *45*(1), 119–129. https://doi.org/10.1002/EJI.201444651

Martin-Gayo, E., Cronin, J., Hickman, T., Ouyang, Z., Lindqvist, M., Kolb, K. E., Schulze zur Wiesch, J., Cubas, R., Porichis, F., Shalek, A. K., van Lunzen, J., Haddad, E. K., Walker, B. D., Kaufmann, D. E., Lichterfeld, M., & Yu, X. G. (2017). Circulating CXCR5+CXCR3+PD-1lo Tfh-like cells in HIV-1 controllers with neutralizing antibody breadth. *JCI Insight*, *2*(2), e89574. https://doi.org/10.1172/JCI.INSIGHT.89574

Morita, R., Schmitt, N., Bentebibel, S. E., Ranganathan, R., Bourdery, L., Zurawski, G., Foucat, E., Dullaers, M., Oh, S. K., Sabzghabaei, N., Lavecchio, E. M., Punaro, M., Pascual, V., Banchereau, J., & Ueno, H. (2011). Human Blood CXCR5+CD4+ T Cells Are Counterparts of T Follicular Cells and Contain Specific Subsets that Differentially Support Antibody Secretion. *Immunity*, *34*(1), 108–121. https://doi.org/10.1016/J.IMMUNI.2010.12.012

Nakayamada, S., Kanno, Y., Takahashi, H., Jankovic, D., Lu, K. T., Johnson, T. A., Sun, H. wei, Vahedi, G., Hakim, O., Handon, R., Schwartzberg, P. L., Hager, G. L., & O'Shea, J. J. (2011). Early Th1 Cell Differentiation Is Marked by a Tfh Cell-like Transition. *Immunity*, *35*(6), 919–931. https://doi.org/10.1016/J.IMMUNI.2011.11.012

Nguyen, C., Kudek, M., Zander, R., Niu, H., Shen, J., Bauer, A., Alson, D., Khatun, A., Chen, Y., Sun, J., Drobyski, W., Edelson, B. T., & Cui, W. (2024). Bhlhe40 Promotes CD4+ T Helper 1 Cell and Suppresses T Follicular Helper Cell Differentiation during Viral Infection. *Journal of Immunology (Baltimore, Md. : 1950)*, *212*(11), 1829–1842. https://doi.org/10.4049/JIMMUNOL.2300355

Oestreich, K. J., Mohn, S. E., & Weinmann, A. S. (2012). Molecular mechanisms that control the expression and activity of Bcl-6 in TH1 cells to regulate flexibility with a TFH-like gene profile. *Nature Immunology 2012 13:4*, *13*(4), 405–411. https://doi.org/10.1038/ni.2242

Oosterhuis, K., Aleyd, E., Vrijland, K., Schumacher, T. N., & Haanen, J. B. (2012). Rational Design of DNA Vaccines for the Induction of Human Papillomavirus Type 16 E6- and E7-Specific Cytotoxic T-Cell Responses. *Human Gene Therapy*, *23*(12), 1301–1312. https://doi.org/10.1089/hum.2012.101

O'Shea, J., & Paul, W. E. (2010). Mechanisms underlying lineage commitment and plasticity of helper CD4+ T cells. *Science (New York, N.Y.)*, *327*(5969), 1098–1102. https://doi.org/10.1126/SCIENCE.1178334

875 Osum, K. C., & Jenkins, M. K. (2023). Toward a general model of CD4+ T cell subset specification
876 and memory cell formation. *Immunity*, *56*(3), 475–484.
877 https://doi.org/10.1016/J.IMMUNI.2023.02.010

878 Rice, J., Elliott, T., Buchan, S., & Stevenson, F. K. (2001). DNA fusion vaccine designed to induce
879 cytotoxic T cell responses against defined peptide motifs: implications for cancer vaccines.
880 *Journal of Immunology (Baltimore, Md. : 1950)*, *167*(3), 1558–1565.
881 https://doi.org/10.4049/JIMMUNOL.167.3.1558

882 Schorer, M., Kuchroo, V. K., & Joller, N. (2019). Role of co-stimulatory molecules in T helper cell
883 differentiation. *Advances in Experimental Medicine and Biology*, *1189*, 153–177.
884 https://doi.org/10.1007/978-981-32-9717-3_6

885 Schulz, O., Edwards, A. D., Schito, M., Aliberti, J., Manickasingham, S., Sher, A., & Reis e Sousa, C.
886 (2000). CD40 triggering of heterodimeric IL-12 p70 production by dendritic cells in vivo requires
887 a microbial priming signal. *Immunity*, *13*(4), 453–462. https://doi.org/10.1016/S1074-
888 7613(00)00045-5

889 Setty, M., Tadmor, M. D., Reich-Zeliger, S., Angel, O., Salame, T. M., Kathail, P., Choi, K., Bendall,
890 S., Friedman, N., & Pe'Er, D. (2016). Wishbone identifies bifurcating developmental trajectories
891 from single-cell data. *Nature Biotechnology*, *34*(6), 637–645. https://doi.org/10.1038/NBT.3569

892 Shaw, L. A., Bélanger, S., Omilusik, K. D., Cho, S., Scott-Browne, J. P., Nance, J. P., Goulding, J.,
893 Lasorella, A., Lu, L. F., Crotty, S., & Goldrath, A. W. (2016). Id2 reinforces TH1 differentiation
894 and inhibits E2A to repress TFH differentiation. *Nature Immunology*, *17*(7), 834–843.
895 https://doi.org/10.1038/NI.3461

896 Sheikh, A. A., & Groom, J. R. (2021). Transcription tipping points for T follicular helper cell and T-
897 helper 1 cell fate commitment. *Cellular & Molecular Immunology*, *18*(3), 528–538.
898 https://doi.org/10.1038/S41423-020-00554-Y

899 Shin, C., Han, J. A., Koh, H., Choi, B., Cho, Y., Jeong, H., Ra, J. S., Sung, P. S., Shin, E. C., Ryu,
900 S., & Do, Y. (2015). CD8α− Dendritic Cells Induce Antigen-Specific T Follicular Helper Cells
901 Generating Efficient Humoral Immune Responses. *Cell Reports*, *11*(12), 1929–1940.
902 https://doi.org/10.1016/J.CELREP.2015.05.042

903 Simms, P. E., & Ellis, T. M. (1996). Utility of flow cytometric detection of CD69 expression as a rapid
904 method for determining poly- and oligoclonal lymphocyte activation. *Clinical and Diagnostic*
905 *Laboratory Immunology*, *3*(3), 301–304. https://doi.org/10.1128/CDLI.3.3.301-304.1996

906 Song, W., & Craft, J. (2024). T Follicular Helper Cell Heterogeneity. *Annual Review of Immunology*,
907 *42*(1), 127–152. https://doi.org/10.1146/ANNUREV-IMMUNOL-090222-102834

908 Tubo, N. J., Pagán, A. J., Taylor, J. J., Nelson, R. W., Linehan, J. L., Ertelt, J. M., Huseby, E. S.,
909 Way, S. S., & Jenkins, M. K. (2013). Single Naive CD4+ T Cells from a Diverse Repertoire
910 Produce Different Effector Cell Types during Infection. *Cell*, *153*(4), 785–796.
911 https://doi.org/10.1016/J.CELL.2013.04.007

912 Vinuesa, C. G., Linterman, M. A., Yu, D., & Maclennan, I. C. M. (2016). Follicular Helper T Cells.
913 *Annual Review of Immunology*, *34*, 335–368. https://doi.org/10.1146/ANNUREV-IMMUNOL-
914 041015-055605

915 Wang, C. J., Heuts, F., Ovcinnikovs, V., Wardzinski, L., Bowers, C., Schmidt, E. M., Kogimtzis, A.,
916 Kenefeck, R., Sansom, D. M., Walker, L. S. K., & Weiss, A. (2015). CTLA-4 controls follicular
917 helper T-cell differentiation by regulating the strength of CD28 engagement. *Proceedings of the*

National Academy of Sciences of the United States of America, *112*(2), 524–529. https://doi.org/10.1073/PNAS.1414576112

Weinstein, J. S., Laidlaw, B. J., Lu, Y., Wang, J. K., Schulz, V. P., Li, N., Herman, E. I., Kaech, S. M., Gallagher, P. G., & Craft, J. (2018). STAT4 and T-bet control follicular helper T cell development in viral infections. *Journal of Experimental Medicine*, *215*(1), 337–355. https://doi.org/10.1084/JEM.20170457

Wu, R., & Murphy, K. M. (2022). DCs at the center of help: Origins and evolution of the three-cell-type hypothesis. *The Journal of Experimental Medicine*, *219*(7). https://doi.org/10.1084/JEM.20211519

Wu, R., Ohara, R. A., Jo, S., Liu, T. T., Ferris, S. T., Ou, F., Kim, S., Theisen, D. J., Anderson, D. A., Wong, B. W., Gershon, T., Schreiber, R. D., Murphy, T. L., & Murphy, K. M. (2022). Mechanisms of CD40-dependent cDC1 licensing beyond costimulation. *Nature Immunology*, *23*(11), 1536–1550. https://doi.org/10.1038/S41590-022-01324-W

Xia, Y., Sandor, K., Pai, J. A., Daniel, B., Raju, S., Wu, R., Hsiung, S., Qi, Y., Yangdon, T., Okamoto, M., Chou, C., Hiam-Galvez, K. J., Schreiber, R. D., Murphy, K. M., Satpathy, A. T., & Egawa, T. (2022). BCL6-dependent TCF-1+ progenitor cells maintain effector and helper CD4+ T cell responses to persistent antigen. *Immunity*, *55*(7), 1200-1215.e6. https://doi.org/10.1016/J.IMMUNI.2022.05.003

Xu, W., Zhao, X., Wang, X., Feng, H., Gou, M., Jin, W., Wang, X., Liu, X., & Dong, C. (2019). The Transcription Factor Tox2 Drives T Follicular Helper Cell Development via Regulating Chromatin Accessibility. *Immunity*, *51*(5), 826-839.e5. https://doi.org/10.1016/J.IMMUNI.2019.10.006

Yin, X., Chen, S., & Eisenbarth, S. C. (2021). Dendritic Cell Regulation of T Helper Cells. *Annual Review of Immunology*, *39*, 759–790. https://doi.org/10.1146/ANNUREV-IMMUNOL-101819-025146

Zheng, L., Qin, S., Si, W., Wang, A., Xing, B., Gao, R., Ren, X., Wang, L., Wu, X., Zhang, J., Wu, N., Zhang, N., Zheng, H., Ouyang, H., Chen, K., Bu, Z., Hu, X., Ji, J., & Zhang, Z. (2021). Pan-cancer single-cell landscape of tumor-infiltrating T cells. *Science (New York, N.Y.)*, *374*(6574). https://doi.org/10.1126/SCIENCE.ABE6474

Zou, D., Yin, Z., Yi, S. G., Wang, G., Guo, Y., Xiao, X., Li, S., Zhang, X., Gonzalez, N. M., Minze, L. J., Wang, L., Wong, S. T. C., Osama Gaber, A., Ghobrial, R. M., Li, X. C., & Chen, W. (2024). CD4+ T cell immunity is dependent on an intrinsic stem-like program. *Nature Immunology*, *25*(1), 66–76. https://doi.org/10.1038/S41590-023-01682-Z

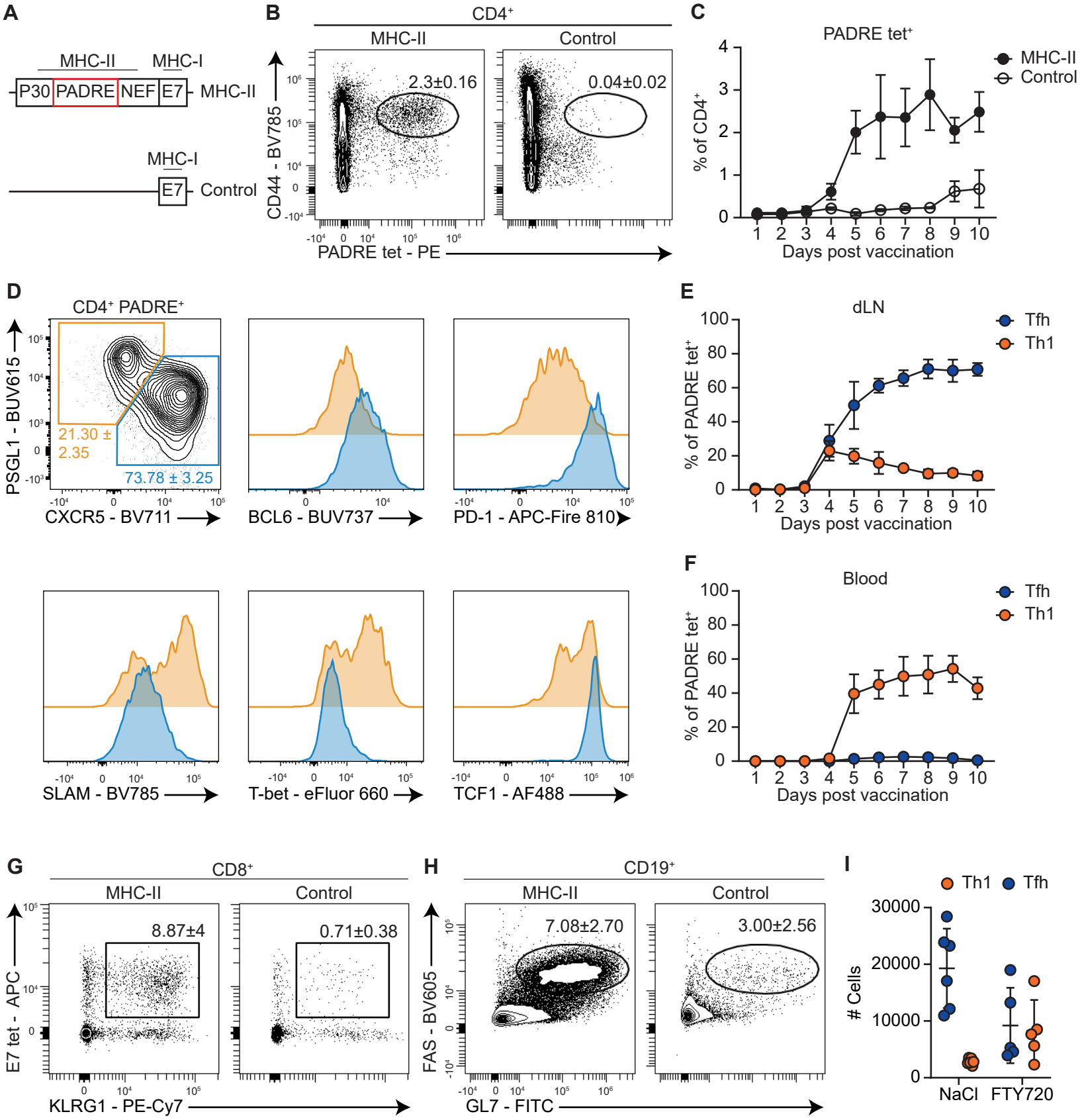

Figure 1: A vaccination model to study differentiation of vaccine-primed CD4 T cells into Th1 and Tfh cells.
A) Scheme of epitopes in MHC-II and control DNA vaccines. B) Representative flow cytometry plots depicting frequency of CD44$^+$ PADRE tet$^+$ CD4 T cells in dLN at day 5 post-vaccination (N=3, mean ± SD). C) Frequency of PADRE tet$^+$ CD4 T cells in dLN over time (N=8 for MHC-II, N=3 for Control). D) Representative flow cytometry plots depicting the phenotype of PADRE tet$^+$ CD4 T cells in the dLN at day 8 post-vaccination. Colors in histograms match the CXCR5$^-$ PSGL1^{hi} (orange) or CXCR5$^+$ PSGL1^{mid-lo} (blue) populations E, F) Frequency of Tfh (CXCR5$^+$ PSGL1^{lo} PD-1$^+$ BCL6$^+$) and Th1 cells (CXCR5$^-$ PSGL1^{hi} T-bet$^+$ SLAM$^+$) within PADRE tet$^+$ CD4 T cells in dLN (E) or blood (F) over time after MHC-II-vaccination (N=5). G) Representative contour plots depicting antigen-specific effector CD8 T cells (E7 tet$^+$ KLRG1$^+$) in blood at day 10 after MHC-II or control vaccination. H) Representative contour plots depicting GL7$^+$ FAS$^+$ GC B cells in the dLN at day 8 after MHC-II or control vaccination. I) Absolute numbers of Th1 and Tfh PADRE tet$^+$ CD4 T cells in dLN at d7 post vaccination (N=6 mean ± SD).

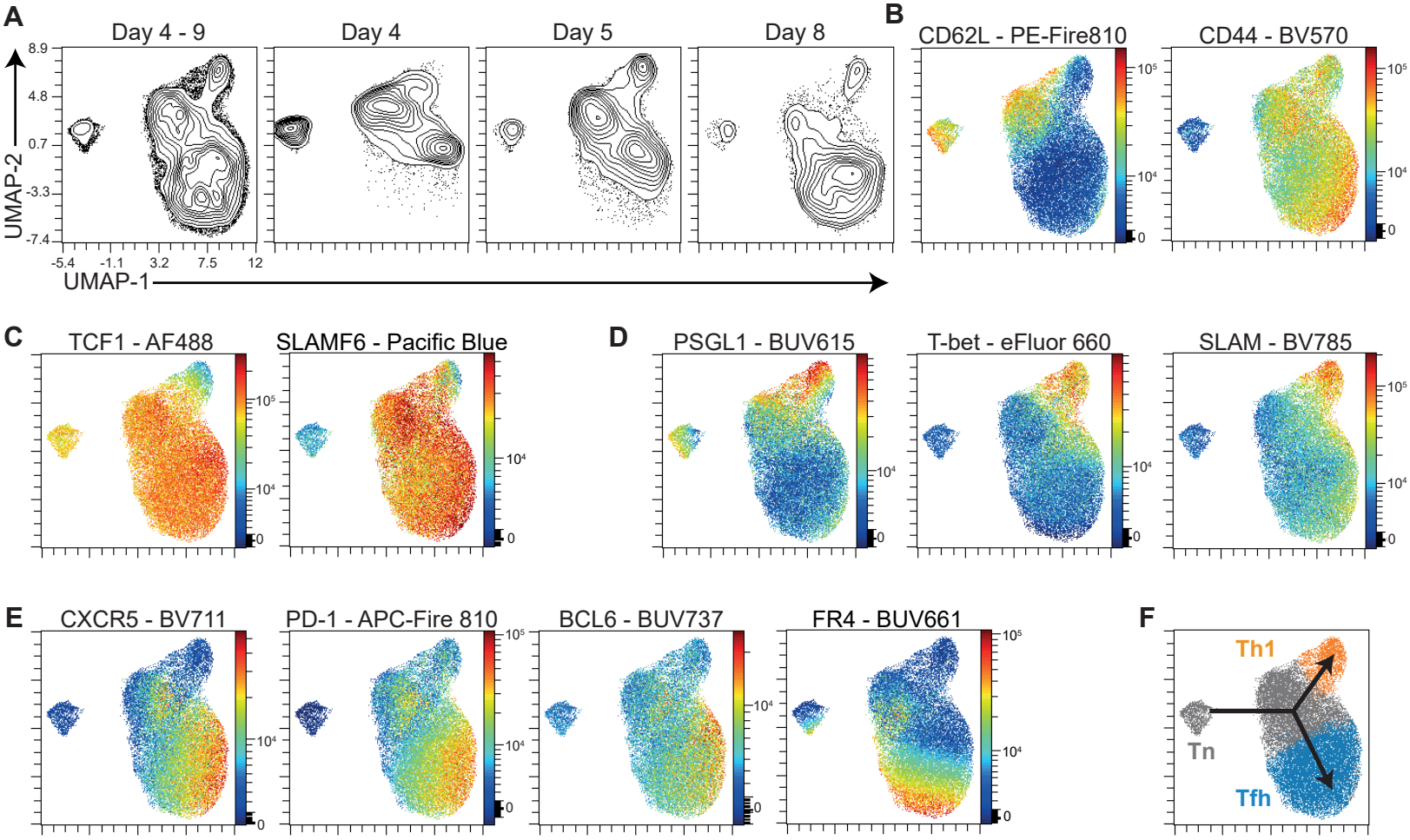

Figure 2: Temporal analysis highlights a common differentiation branchpoint for Th1 and Tfh cells.
A) UMAP projections showing concatenated PADRE tet⁺ CD4 T cells in dLN from day 4-9 post-vaccination, or single projections at days 4, 5 or 8 (N=5 per time point). B-E) Overlay of CD62L and CD44 (B), TCF1 and SLAMF6 (C), PSGL1, T-bet and SLAM (D) and CXCR5, PD-1, BCL6 and FR4 expression (E). F) Overlay of Wishbone branching on UMAP from panel D. Arrows depict differentiation branches. Grey: trunk; orange: branch 1, identified as Th1 cells; blue: branch 2, identified as Tfh cells.

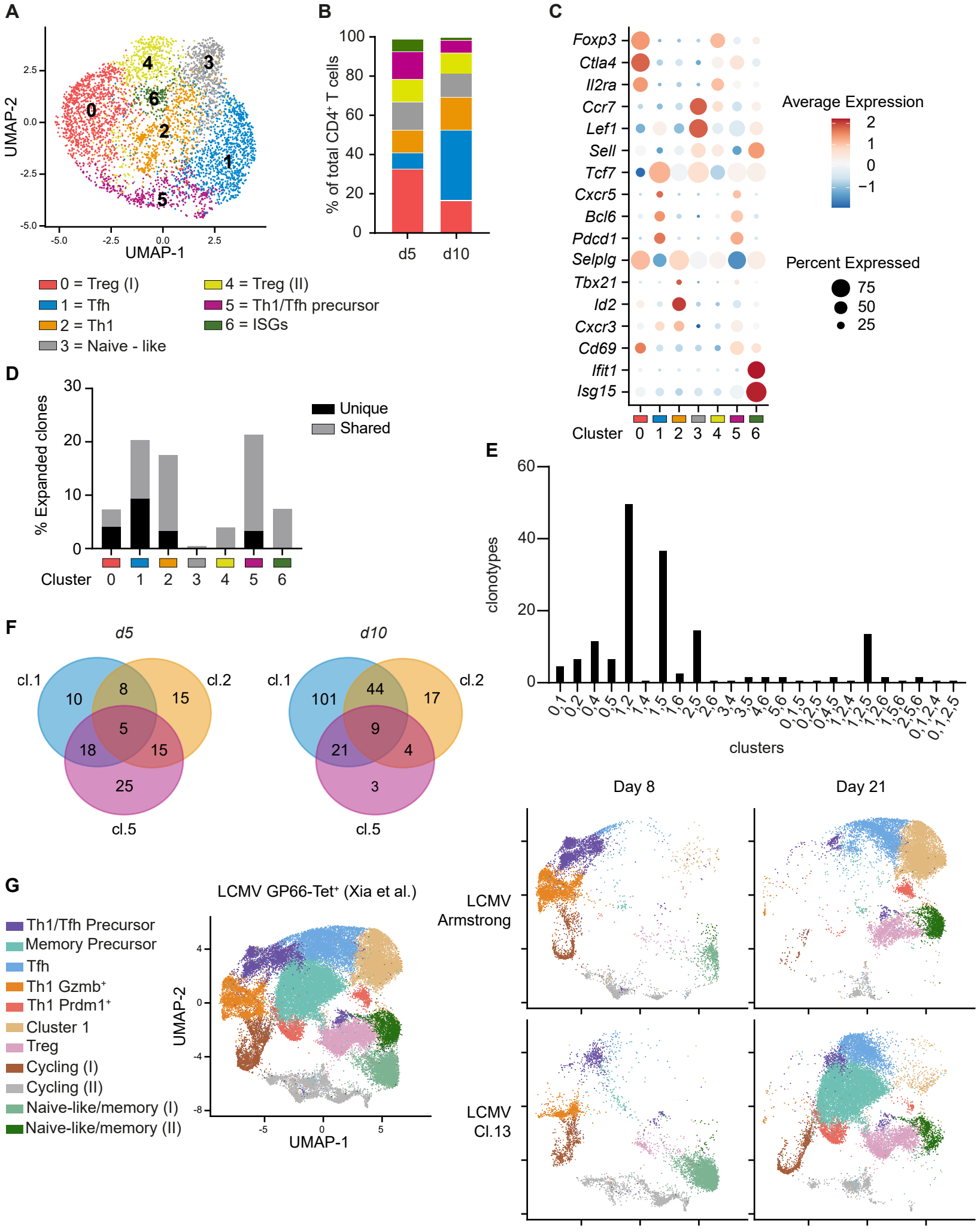
A
UMAP-2
UMAP-1
0 = Treg (I)
1 = Tfh
2 = Th1
3 = Naive - like
4 = Treg (II)
5 = Th1/Tfh precursor
6 = ISGs
B
% of total CD4+ T cells
d5
d10
C
Foxp3
Ctla4
Il2ra
Ccr7
Lef1
Sell
Tcf7
Cxcr5
Bcl6
Pdcd1
Selplg
Tbx21
Id2
Cxcr3
Cd69
Ifit1
Isg15
Cluster
Average Expression
Percent Expressed
D
% Expanded clones
Unique
Shared
E
clonotypes
clusters
F
d5
d10
cl.1
cl.2
cl.5
G
LCMV GP66-Tet+ (Xia et al.)
Th1/Tfh Precursor
Memory Precursor
Tfh
Th1 Gzmb+
Th1 Prdm1+
Cluster 1
Treg
Cycling (I)
Cycling (II)
Naive-like/memory (I)
Naive-like/memory (II)
Day 8
Day 21
LCMV Armstrong
LCMV Cl.13

Figure 3: Identification of a common precursor of Th1 and Tfh cells.
A) UMAP projection of CD4 T-cell clusters identified by scRNAseq of $CD3^+$ $CD44^+$ $CD62L^-$ T cells isolated from the dLN of mice at days 5 and 10 after vaccination with the MHC-II plasmid. B) Bar plot depicting cluster distribution per time point. C) Average mRNA expression level of indicated differentiation-associated genes and percentage of positive cells per cluster. D) Frequency of expanded TCR clones (>1 cell per clone) per cluster. Black: TCR clones unique to one cluster; grey: TCR clones shared between two or more clusters. E) Quantification of clonotypes shared between two or more indicated clusters. F) Venn diagram depicting TCR sharing between indicated numbers of Tfh cells from cluster (cl.) 1, Th1 cells from cluster 2 and precursor cells from cluster 5 derived from dLN at day 5 (left) or day 10 (right) after vaccination. G) UMAP projection of LCMV-specific splenic CD4 T-cell clusters derived from LCMV-Armstrong and LCMV-clone 13 at day 8 and day 21 post infection from (Xia et al., 2022). Total cells (left). Deconvolution of UMAPs per infection type and day post infection is displayed on the right.

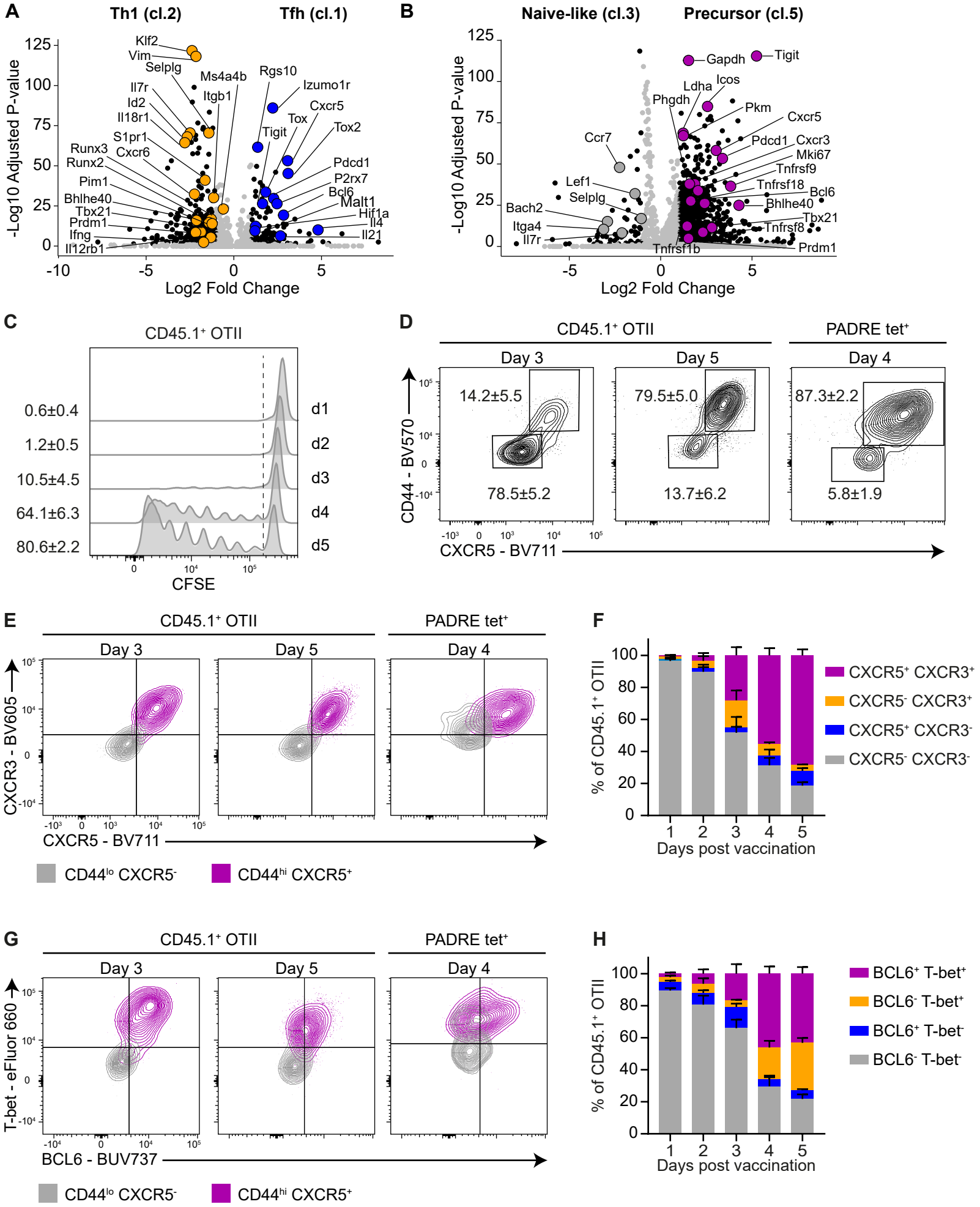
A
Th1 (cl.2)
Tfh (cl.1)
-Log10 Adjusted P-value
Log2 Fold Change
Klf2
Vim
Selplg
Ms4a4b
Il7r
Itgb1
Id2
Il18r1
S1pr1
Runx3
Cxcr6
Runx2
Pim1
Bhlhe40
Tbx21
Prdm1
Ifng
Il12rb1
Rgs10
Izumo1r
Cxcr5
Tox
Tigit
Tox2
Pdcd1
P2rx7
Bcl6
Malt1
Hif1a
Il4
Il21
B
Naive-like (cl.3)
Precursor (cl.5)
Gapdh
Tigit
Ldha
Icos
Phgdh
Pkm
Cxcr5
Ccr7
Pdcd1
Cxcr3
Mki67
Tnfrsf9
Lef1
Tnfrsf18
Selplg
Bcl6
Bhlhe40
Bach2
Tbx21
Itga4
Tnfrsf8
Il7r
Tnfrsf1b
Prdm1
C
CD45.1⁺ OTII
0.6±0.4
1.2±0.5
10.5±4.5
64.1±6.3
80.6±2.2
d1
d2
d3
d4
d5
CFSE
D
CD45.1⁺ OTII
PADRE tet⁺
Day 3
Day 5
Day 4
14.2±5.5
78.5±5.2
79.5±5.0
13.7±6.2
87.3±2.2
5.8±1.9
CD44 - BV570
CXCR5 - BV711
E
CD45.1⁺ OTII
PADRE tet⁺
Day 3
Day 5
Day 4
CXCR3 - BV605
CXCR5 - BV711
CD44lo CXCR5-
CD44hi CXCR5+
F
% of CD45.1⁺ OTII
Days post vaccination
CXCR5⁺ CXCR3⁺
CXCR5⁻ CXCR3⁺
CXCR5⁺ CXCR3⁻
CXCR5⁻ CXCR3⁻
G
CD45.1⁺ OTII
PADRE tet⁺
Day 3
Day 5
Day 4
T-bet - eFluor 660
BCL6 - BUV737
CD44lo CXCR5-
CD44hi CXCR5+
H
% of CD45.1⁺ OTII
Days post vaccination
BCL6⁺ T-bet⁺
BCL6⁻ T-bet⁺
BCL6⁺ T-bet⁻
BCL6⁻ T-bet⁻

Figure 4: Common Th1/Tfh precursors co-express Th1- and Tfh markers at protein level.
A, B) Volcano plots depicting differential gene expression derived from scRNAseq data, comparing Tfh cells (cl. 1) versus Th1 cells (cl. 2) (A), or naive-like CD4 T cells (cl. 3) versus the common Th1/Tfh precursor cells (cl. 5) (B). Black dots depict genes with fold change < -1 or > 1 and adjusted P<0.05. C) Mice received OTII cells and MHC-II:OVA vaccine and dLNs were harvested and cells analyzed by flow cytometry. Histograms depicting divisions of vaccine-activated, adoptively transferred OTII cells, as measured by CFSE dilution. Numbers indicate frequency of divided OTII cells (mean ± SD). D) Representative CD44 and CXCR5 protein expression on CD45.1^{+} OTII or PADRE tet^{+} CD4 T cells, measured in dLNs at indicated days post-vaccination. E, G) Representative overlays of CXCR5 and CXCR3 (E) or T-bet and BCL6 (G) protein expression in CD44^{lo} CXCR5^{-} (gray) and CD44^{+} CXCR5^{+} (purple) CD45.1^{+} OTII or PADRE tet^{+} CD4 T cells. F, H) Proportion of CD45.1^{+} OTII responder cells expressing CXCR5 and CXCR3 (F) or T-bet and BCL6 (H) in the dLNs at the indicated days post-vaccination (N=3-5 per time point; representative of 3 independent experiments). Graphs depict mean ± SD.

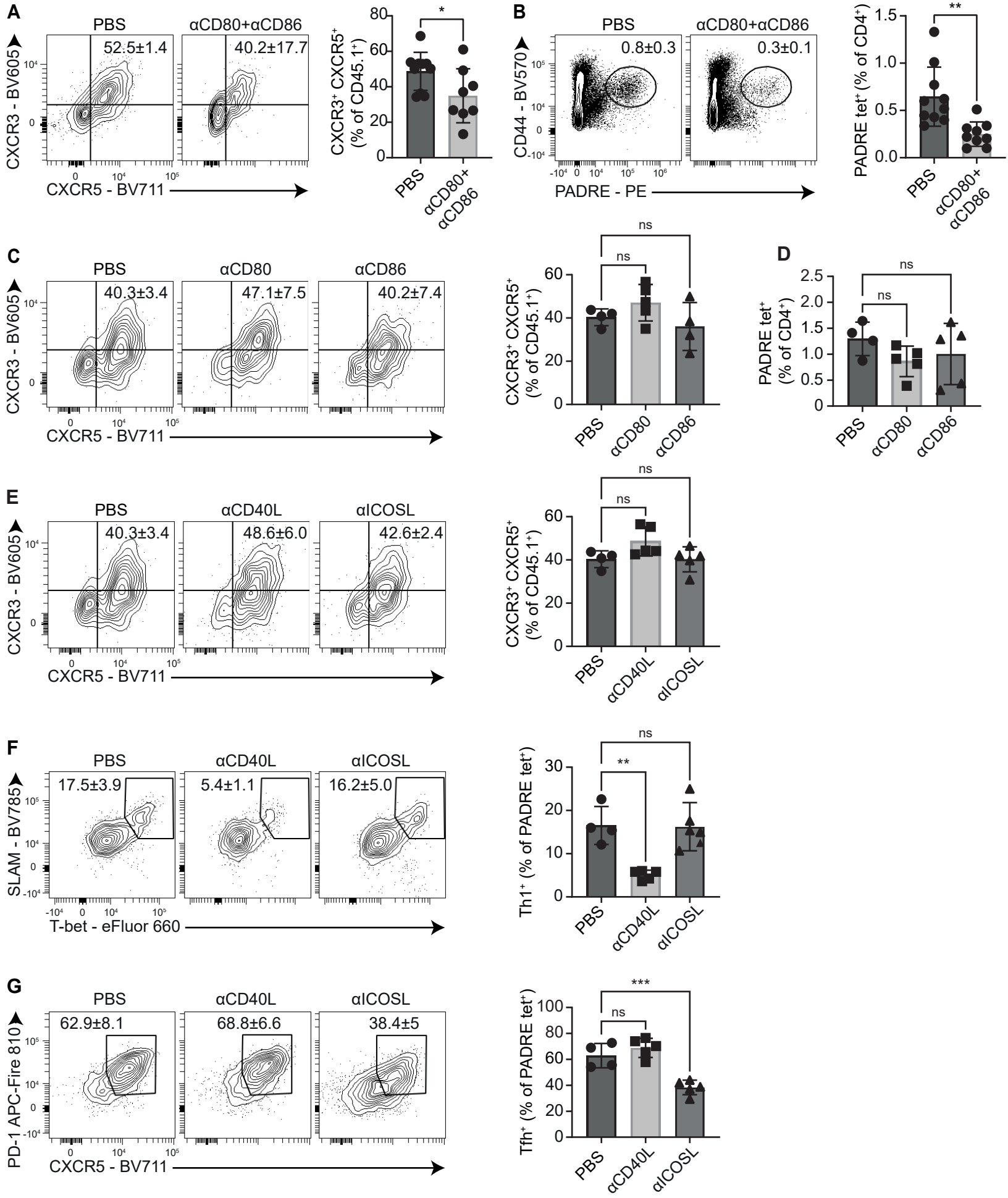
A
PBS
αCD80+αCD86
52.5±1.4
40.2±17.7
CXCR3 - BV605
CXCR5 - BV711
CXCR3⁺ CXCR5⁺ (% of CD45.1⁺)
*
PBS
αCD80+ αCD86
B
PBS
αCD80+αCD86
0.8±0.3
0.3±0.1
CD44 - BV570
PADRE - PE
PADRE tet⁺ (% of CD4⁺)
**
PBS
αCD80+ αCD86
C
PBS
αCD80
αCD86
40.3±3.4
47.1±7.5
40.2±7.4
CXCR3 - BV605
CXCR5 - BV711
CXCR3⁺ CXCR5⁺ (% of CD45.1⁺)
ns
ns
PBS
αCD80
αCD86
D
PADRE tet⁺ (% of CD4⁺)
ns
ns
PBS
αCD80
αCD86
E
PBS
αCD40L
αICOSL
40.3±3.4
48.6±6.0
42.6±2.4
CXCR3 - BV605
CXCR5 - BV711
CXCR3⁺ CXCR5⁺ (% of CD45.1⁺)
ns
ns
PBS
αCD40L
αICOSL
F
PBS
αCD40L
αICOSL
17.5±3.9
5.4±1.1
16.2±5.0
SLAM - BV785
T-bet - eFluor 660
Th1⁺ (% of PADRE tet⁺)
ns
**
PBS
αCD40L
αICOSL
G
PBS
αCD40L
αICOSL
62.9±8.1
68.8±6.6
38.4±5
PD-1 APC-Fire 810
CXCR5 - BV711
Tfh⁺ (% of PADRE tet⁺)
***
ns
PBS
αCD40L
αICOSL

Figure 5: CD28 costimulation promotes formation of the Th1/Tfh precursor pool, from which CD40 or ICOS drive Th1 or Tfh differentiation, respectively.

Mice received OTII cells and MHC-II:OVA vaccine and were treated with blocking mAbs to indicated costimulatory ligands or PBS (control). At day 5 after vaccination, cells from dLNs were analyzed by flow cytometry. Representative plots and quantification of frequencies of cells with indicated markers are shown. (A, B) Frequencies of CXCR3$^+$ CXCR5$^+$ CD45.1$^+$ OTII cells (A) and PADRE tet$^+$ CD4 T cells in mice treated with a combination of blocking mAbs to CD80 and CD86 (B) (N=9-10 per group; data pooled from 2 independent experiments). Unpaired student's-t test. C, D) Frequencies of CXCR3$^+$ CXCR5$^+$ CD45.1$^+$ OTII cells (C) and PADRE tet$^+$ CD4 T cells (D) in mice treated with blocking mAbs to either CD80 or CD86. E) Frequencies of CXCR3$^+$ CXCR5$^+$ precursor CD45.1$^+$ OTII T cells in mice treated with blocking mAb to either CD40L or ICOSL F, G) Frequencies of SLAM$^+$ T-bet$^+$ Th1 (F) and CXCR5$^+$ PD-1$^+$ Tfh (G) PADRE tet$^+$ CD4 T cells in mice treated with blocking mAb to either CD40L or ICOSL. C-G) N=4-5 per group; data are representative at least two independent experiments. One-Way ANOVA with Dunnett post hoc test was used to correct for multiple testing when comparing inhibitory conditions to control. All graphs depict mean ± SD.

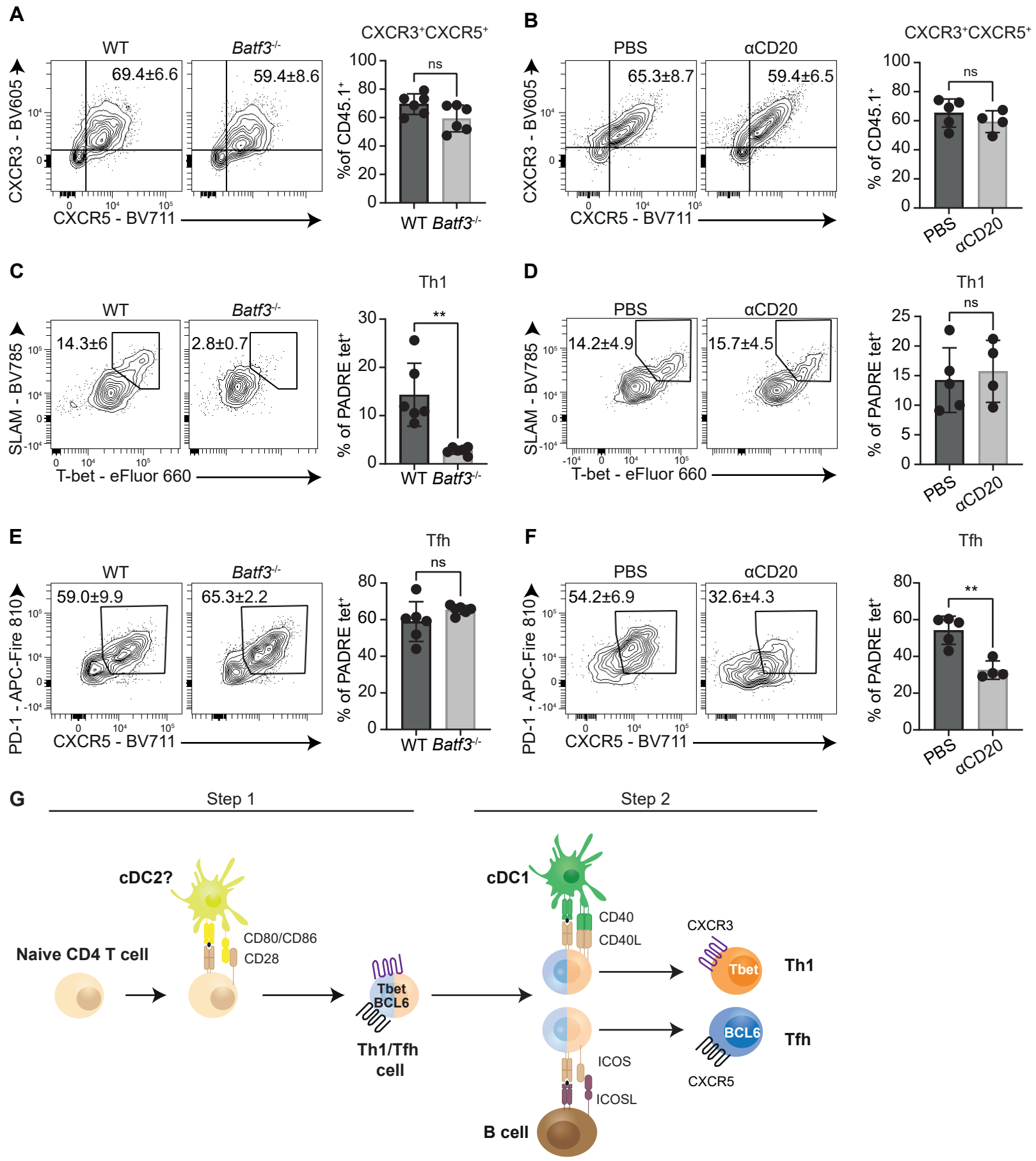
A
WT
Batf3-/-
69.4±6.6
59.4±8.6
CXCR3 - BV605
CXCR5 - BV711
CXCR3+CXCR5+
%of CD45.1+
ns
WT Batf3-/-
B
PBS
αCD20
65.3±8.7
59.4±6.5
% of CD45.1+
C
14.3±6
2.8±0.7
SLAM - BV785
T-bet - eFluor 660
Th1
% of PADRE tet+
**
D
14.2±4.9
15.7±4.5
E
59.0±9.9
65.3±2.2
PD-1 - APC-Fire 810
Tfh
F
54.2±6.9
32.6±4.3
G
Step 1
Step 2
cDC2?
Naive CD4 T cell
CD80/CD86
CD28
Tbet
BCL6
Th1/Tfh cell
cDC1
CD40
CD40L
CXCR3
Th1
Tfh
ICOS
ICOSL
CXCR5
B cell

Figure 6: Th1 or Tfh differentiation from the common Th1/Tfh precursor is driven by interactions with cDC1s or B cells, respectively.

Wild-type (WT) or Batf3-/- mice received OTII cells and MHC-II:OVA vaccine and were treated with depleting mAb to CD20 or control (PBS) as indicated. At day 5 after vaccination, cells from dLN were analyzed by flow cytometry. Representative plots and quantification of frequencies of cells with indicated markers are shown. (A, B) Flow cytometry plots and quantification of CXCR3^{+} CXCR5^{+} CD45.1^{+} OTII cells in the dLN of WT versus *Batf3*$^{-/-}$ mice (A), or WT mice that were treated with B-cell depleting anti-CD20 mAb or PBS (control), two days before vaccination (B). C-F) Flow cytometry plots and quantification of SLAM^{+}T-bet^{+} Th1 (C, D) or CXCR5^{+} PD-1^{+} Tfh (E, F) PADRE tet^{+} CD4 T cells in WT versus *Batf3*$^{-/-}$ mice (C, E), or WT mice treated with anti-CD20 mAb or PBS (D, F). All graphs depict mean ± SD (N=6 per group in A, C, E; N=4-5 per group in B, D, F). A-F, Unpaired student's t-test. G) Proposed model of cellular and molecular interactions that, next to TCR/CD3 signals, drive CD4 T-cell differentiation towards Th1 or Tfh cells.